Order Number 1343690

The viability of shaped BPSK modulation techniques with 5kHz UHF SATCOM channels

Fox, Michael Ethan, M.S.

The University of Arizona, 1991

U·M·I
300 N. Zeeb Rd.
Ann Arbor, MI 48106

THE VIABILITY OF SHAPED BPSK MODULATION TECHNIQUES WITH 5KHZ UHF SATCOM CHANNELS

by

Michael Ethan Fox

A Thesis Submitted to the Faculty of the

DEPARTMENT OF ELECTRICAL AND COMPUTER ENGINEERING

In Partial Fulfillment of the Requirements

For the Degree of

MASTER OF SCIENCE

WITH A MAJOR IN ELECTRICAL ENGINEERING

In the Graduate College

THE UNIVERSITY OF ARIZONA

1 9 9 1

STATEMENT BY AUTHOR

This thesis has been submitted in partial fulfillment of requirements for an advanced degree at The University of Arizona and is deposited in the University Library to be made available to borrowers under rules of the library.

Brief quotations from this thesis are allowable without special permission, provided that accurate acknowledgment of source is made. Requests for permission for extended quotation from or reproduction of this manuscript in whole or in part may be granted by the head of the major department or the Dean of the Graduate College when in his or her judgment the proposed use of the material is in the interests of scholarship. In all other instances, however, permission must be obtained from the author.

SIGNED: Michael E Fox

APPROVAL BY THESIS DIRECTOR

This thesis has been approved on the date shown below:

Michael W. Marcellin
Assistant Professor of
Electrical and Computer Engineering

1 March 1991
Date

To my parents

ACKNOWLEDGMENTS

Working on my Master's thesis was a very interesting and satisfying experience that was made possible by the advice and support of a number of people. First of all, I would like to thank Dr. Michael W. Marcellin. His leadership, encouragement, and technical advice made this work possible. I am also grateful to the master's committee members, Dr. Randall K. Bahr and Dr. Pamela Nielsen, for reviewing my thesis.

I would like to thank WaveLogic Corporation for funding this work and for providing the neccessary tools to carry it out. In particular, I would like to acknowledge Keith M. Kumm and Mark R. Jensen of WaveLogic Corp. Their technical assistance and encouragement are greatly appreciated.

Finally, I would like to thank my family, friends and colleagues for their moral support in bringing all my work together.

TABLE OF CONTENTS

LIST OF FIGURES 6

LIST OF TABLES 8

ABSTRACT 9

1. Introduction 10
1.1. Background 10
1.2. Existing Shaped BPSK Modulations with Constant Amplitude Envelopes 15
1.3. Research Objectives 19

2. Shaped BPSK: A Class of BPSK/CPM Hybrid Modulations 21
2.1. Constant Amplitude Signals 21
2.2. BPSK 22
2.3. CPM 25
2.4. BPSK/CPM Hybrid Modulations 26
2.4.1. JCS SBPSK 27
2.4.2. Dapper and Hill SBPSK 27
2.4.3. Generalized Dapper and Hill SBPSK 29
2.5. Examples of SBPSK Waveforms 30

3. Spectral Characteristics of SBPSK Signals 40
3.1. Evaluation of Power Spectral Density 40
3.2. Power Spectral Densities of SBPSK Modulations 45
3.3. Spectral Efficiency of SBPSK Modulations 51

4. Performance of SBPSK Modulations 57
4.1. Probability of Error 57
4.2. Pe for Bandpass Hardlimited SBPSK 71
4.3. In-Band Signal-to-Noise Ratio (SNR_I) 77

5. Summary and Conclusions 82
5.1. Summary 82
5.2. Topics for Future Research 83
5.3. Recommended SBPSK Waveform 84

REFERENCES 88

LIST OF FIGURES

1.1. A Digital Communication System for Analog Signals 11
1.2. The Digital Channel Model 12
1.3. PSD of 2400 bps BPSK and the JCS Adjacent Channel Interference Constraint . . 14
1.4. JCS SBPSK Modulation Format 16
1.5. 50% Dapper and Hill SBPSK Modulation Format 17
1.6. Modulation format for Modified BPSK by Yazdani et al. 18

2.1. State Diagram for $U_{\text{D\&H SBPSK}}$ 28
2.2. BPSK Sample Waveforms. 33
2.3. JCS SBPSK Sample Waveforms. 34
2.4. 50% Dapper and Hill SBPSK Sample Waveforms. 35
2.5. 50% Sin SBPSK Sample Waveforms. 36
2.6. 50% Hamming SBPSK Sample Waveforms. 37
2.7. 50% Min. 3 Term Blackman SBPSK Sample Waveforms. 38
2.8. 50% Tukey 75% Rolloff SBPSK Sample Waveforms. 39

3.1. BPSK Power Spectral Densities via Computer Simulation. 44
3.2. Power Spectral Densities of SBPSK Modulations. 46
3.3. Power Spectral Densities of SBPSK Modulations (cont.). 47
3.4. PSD of 2400 bps JCS SBPSK and the JCS Spectral Constraint 48
3.5. PSD of 2400 bps 50% D&H SBPSK and the JCS Spectral Constraint 49
3.6. PSD of 3600 bps 50% D&H SBPSK and the JCS Spectral Constraint 50
3.7. PSD of 2400 bps 50% D&H SBPSK with a Carrier EIRP of 22 dBW and the JCS Spectral Constraint 50
3.8. The Definition of One-Sided Bandwidth, B. 51
3.9. Fractional Out-of-Band Power for Various SBPSK Modulations. 53
3.10. Fractional Out-of-Band Power for Bandpass Hardlimited SBPSK. 55
3.11. Fractional Out-of-Band Power for Bandpass Hardlimited SBPSK (cont.). 56

4.1. A Simple Channel Model. 58
4.2. A Block Diagram of the Optimum BPSK Demodulator. 58
4.3. Ideal Timing Recovery for BPSK Signaling. 60
4.4. Ideal Timing Recovery for SBPSK Signaling. 60
4.5. Piecewise Calculation of $\mathbf{X}_i$ for SBPSK Signals. 63
4.6. Pe for BPSK and Various SBPSK Modulations. 70
4.7. A Model of a Typical Satellite Transponder with Downlink AWGN. 71
4.8. Pe for Bandpass Hardlimited BPSK and SBPSK Signals. 73
4.9. Pe for Bandpass Hardlimited BPSK and SBPSK Signals (cont.). 74
4.10. Pe vs. Phase Reference Error for Bandpass Hardlimited BPSK and SBPSK Signals. 75

4.11. Pe for Bandpass Hardlimited BPSK and SBPSK Signals w/ 10° Phase Reference Error. 76
4.12. Assumed Channel Spacing for Adjacent Channel Interference Analysis. 79
4.13. SNR_I for BPSK and SBPSK Signals as a Function of λ. 80

5.1. Complete 5 kHz SATCOM Channel System. 86

LIST OF TABLES

1.1. JCS Spectral Constraint 14

2.1. Parameters for Selected Constant Amplitude Signals 31
2.2. Pulse Shapes for Selected Generalized D&H Modulations 32

ABSTRACT

A method of generating constant envelope BPSK compatible modulation formats is described in which spectral containment is achieved via controlled phase rotations. These Shaped BPSK modulations can be considered BPSK/CPM hybrids. The instantaneous phase transitions of BPSK are tempered to become the continuous phase rotations of CPM.

The SBPSK modulations described above are compared with classical BPSK as well as a Shaped BPSK modulation specified by the Joint Chiefs of Staff for use with Department of Defense 5kHz UHF SATCOM channels. It is shown that the use of SBPSK modulations can allow significant increases in the data transmission rate without exceeding the spectral "envelope" of a lower rate BPSK signal. Analysis also includes fractional out of band power curves for the modulated signals before and after transmission through a bandpass hard-limited channel. Equivalent SNR's are generated to quantify the simultaneous effects of decreased adjacent channel interference at the expense of I channel energy. Finally, probability of error curves vs SNR are presented for BPSK and SBPSK modulations transmitted through a band-limited and hard-limited channel.

CHAPTER 1

Introduction

1.1 Background

In recent times, digital transmission of information has come to dominate the design of communication systems. Certainly a driving factor has been the proliferation of computers into the workplace and the home. The resulting explosion in computer-to-computer communication is inherently digital. Equally important is the widespread use of digital communications for transmission of analog signals such as voice and images. Digital transmission of analog signals is motivated by the ability to regenerate, multiplex, and switch digital signals. Figure 1.1 demonstrates the use of a digital transmission system with an analog signal.

In this figure, the signal $m(t)$ originates from an analog source. Prefiltering and analog-to-digital conversion is performed on $m(t)$ yielding the binary sequence x_i. Prefiltering insures that $m(t)$ is bandlimited, while analog-to-digital conversion provides discrete samples of $m(t)$. The frequency of A/D conversion is determined from the sampling theorem which states that a bandlimited waveform can be reconstructed from its samples provided that the sampling rate is at least twice as high as the highest frequency component of the original waveform. The binary sequence x_i is then source coded to remove data redundancy. Source coding is followed by channel coding. The objective of channel coding is to maximize the bit rate at the input of the channel coder that can be transmitted through the channel with a specified fidelity. Channel coding is an extremely general term that may include such codes as error correction codes, run-length-limited codes, and encryption codes. The modulator converts the bit sequence a_i into waveforms suitable for transmission through the

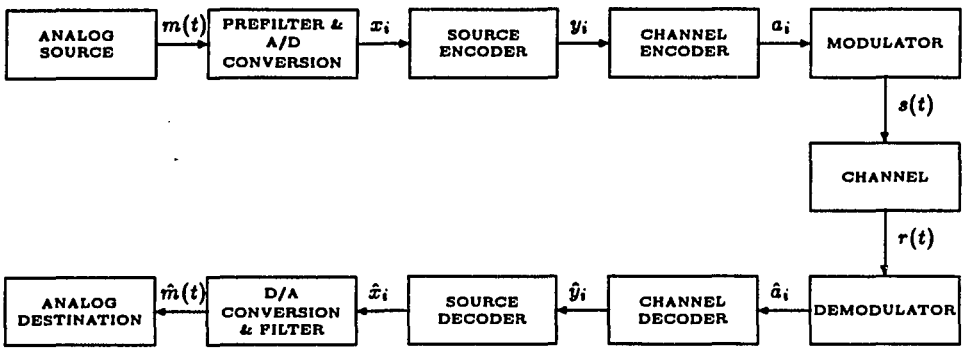

Figure 1.1: A Digital Communication System for Analog Signals

channel. Generally the transmitted signal is degraded by the channel. Therefore, the received signal $r(t)$ will not be identical to $s(t)$. The demodulator attempts to recover the original bit stream a_i. Its estimate, $\hat{a}_i$, is channel decoded and source decoded creating estimates of x_i and y_i, labeled $\hat{x}_i$ and $\hat{y}_i$ respectively. Finally, the bit stream $\hat{x}_i$ undergoes digital-to-analog conversion and filtering to obtain $\hat{m}(t)$, an estimate of $m(t)$. The same steps apply to the transmission of data from a digital source except that the initial "prefiltering & A/D conversion" and the final "D/A conversion & filtering" are not performed. In many cases, the digital transmission system is designed so that it may be used with bit streams derived from either analog or digital sources.

In this thesis only the modulator, channel, and demodulator are investigated. The performance of various modulations is compared when the channel and the demodulator are fixed. The bit sequence $\{a_i\}_{i=-\infty}^{\infty}$ is assumed to be random. From the perspective of the modulator, the a_i represent binary data. The modulator is unaware of the source of the data or any external channel coding. Thus $\{a_i\}_{i=-\infty}^{\infty}$ is referred to as the "binary data stream." Within certain modulators, it will be necessary to further encode the binary data. This is done to reformat the data stream into a sequence compatible with the mathematical representation of the modulator output, $s(t)$. When

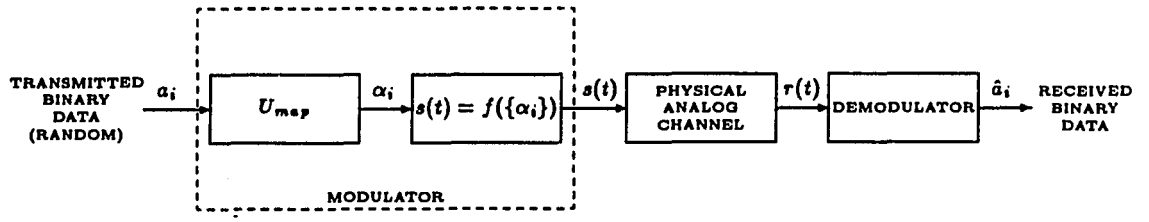

Figure 1.2: The Digital Channel Model

internal coding is necessary, it will be represented as a mapping $U : \{a_i\}_{i=-\infty}^{\infty} \rightarrow \{\alpha_i\}_{i=-\infty}^{\infty}$. The α_i will be referred to as transmitted symbols. In all cases, the modulator input will be a_i, and the demodulator output will be $\hat{a}_i$, an estimate of the binary data stream. Figure 1.2 provides a summary.

The use of digital communications is nowhere more prevalent than in the United States military. Digital satellite communications provides secure, world-wide communication for all branches of the U.S. armed forces. As demand for satellite communications continues to grow, existing "nonprocessed 5 kHz SATCOM channels" have become the subject of increased interest. These satellite channels are characterized by several traits; they are nonprocessed, bandlimited, and hardlimited. Listed below are the definitions of these terms as they apply to the channels of interest:

nonprocessed The channels are capable only of amplifying and retransmitting received signals.

bandlimited Each channel passband is nominally 4 kHz with channel center frequencies only 5 kHz apart.

hardlimited At some point the channel hardlimits the communication signal. A hardlimiter output signal exhibits a fixed amplitude regardless of the amplitude of the input signal, but retains the input signal phase.

In an effort to promote efficient use of these channels, reduce interference between adjacent users, and insure interoperability between terminals, the Joint Chiefs of Staff (JCS) of the United

States military have specified a standard for all terminals accessing the channels [1]. This document specifies that all terminals meet the following criteria:

1. All users support a BPSK interoperable modulation format that will be referred to as Shaped BPSK or *SBPSK*. The terminal must support SBPSK at a data rate of 2400 Hz. Other data rates are permissible as long as the 2400 Hz data rate is supported.

2. Since the channels are hardlimited, the SBPSK modulation must have a constant amplitude envelope.

3. In addition, to limit adjacent channel interference (ACI), the JCS also specify that the spectrum of the modulated signal exhibit the following characteristics:

   - If the equivalent isotropic radiated power (EIRP) of the carrier is less than 18 dBW, then the EIRP (relative to the carrier EIRP) in a 5 kHz band whose center frequency is Δf (kHz) removed from the carrier frequency shall not exceed the values shown in column (1) of Table 1.1.
   - For carrier EIRP levels equal to or greater than 18 dBW, the *maximum* EIRP values shall not exceed those shown in column (2) of Table 1.1.

Figure 1.3 shows that column (1) of Table 1.1 dictates that the spectrum of the SBPSK signal must be contained within the envelope of the spectrum of a 2400 Hz BPSK signal at the same transmitted power. If the SBPSK power spectrum falls off faster than BPSK at 2400 Hz, then the SBPSK signal power may be increased as long as the absolute maximum levels of ACI given in column (2) are not violated. Clearly, the first condition allows the simplest BPSK interoperable modulation (BPSK itself) at the required data rate of 2400 Hz with a maximum carrier EIRP of 18 dBW. The second condition allows any of the following as long as the absolute maximum levels of ACI given in column (2) are not violated:

1. A higher carrier EIRP than 18 dBW at the same bit rate.

Δf (kHz)	Column 1 Relative EIRP (dB)	Column 2 Maximum EIRP (dBW)
5	-13	+5
10	-21	-3
15	-25	-7
20	-28	-10
25	-30	-12
30	-31.5	-13.5
35	-33	-15
40	-34	-16
45	-35	-17
50	-36	-18
55	-37	-19
60	-38	-20
65	-39	-21
$\geq$ 70	-40	-22

Table 1.1: JCS Spectral Constraint

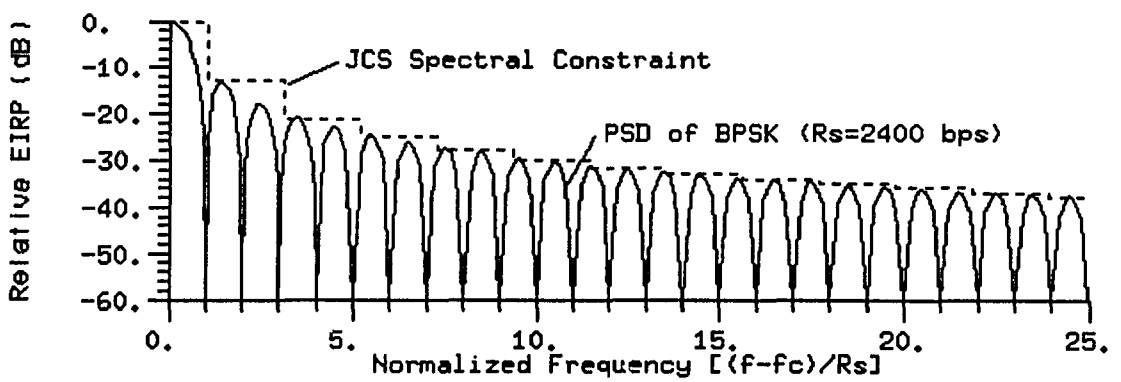

Figure 1.3: PSD of 2400 bps BPSK and the JCS Adjacent Channel Interference Constraint

2. An increased bit rate at the same carrier EIRP.

3. Some combination of the above.

1.2 Existing Shaped BPSK Modulations with Constant Amplitude Envelopes

Several modulation formats have been proposed that accomplish the goal of bandlimiting BPSK while retaining a constant amplitude envelope. The JCS make such a proposal in [1]. The JCS specify a SBPSK modulation format referred to as *JCS SBPSK*. This modulation is characterized by a constant-rate phase transition occurring over 50 percent of a bit period. This phase "rotation" occurs during bits that are inversions of the previous transmitted bit. Thus a change in the polarity of the transmitted data causes the JCS SBPSK modulated signal to rotate to the new value of phase. In addition, the direction of phase vector rotation during a phase transition must always be opposite that of the previous phase rotation. This requirement is motivated by the desire to avoid a net carrier frequency offset. Figure 1.4 illustrates the phase rotations of JCS SBPSK and the corresponding lowpass equivalent in-phase (I) and quadrature (Q) channel signals.

Note that for JCS SBPSK the lowpass Q channel signal is always a half-sine pulse with the same polarity for every phase transition. During transmitted bits that do not require phase transitions the Q channel signal is zero. This results in an average Q channel signal that is non-zero. A Q channel offset will disturb the phase error measurement of a Costas or squaring loop. Thus BPSK demodulators that are not specifically designed for a shaped phase trajectory may be affected.

Dapper and Hill note this in [2] and eliminate the problem in their BPSK interoperable modulation referred to here as *Dapper and Hill SBPSK* or *D&H SBPSK*. D&H SBPSK is nearly identical to JCS SBPSK. There are only two differences:

1. The direction of phase rotation is not always opposite that of the previous phase rotation as in JCS SBPSK. Instead, the phase is allowed to rotate in the same direction twice consecutively. The following two rotations are then in the opposite direction. This allows use of the entire

JCS defines SBPSK as:

- o Data bit transitions are realized by a constant rate, linear phase rotation occurring over 50 % of a symbol period.
- o The direction of the phase vector rotation during a phase transition must be opposite that of the previous phase transition.

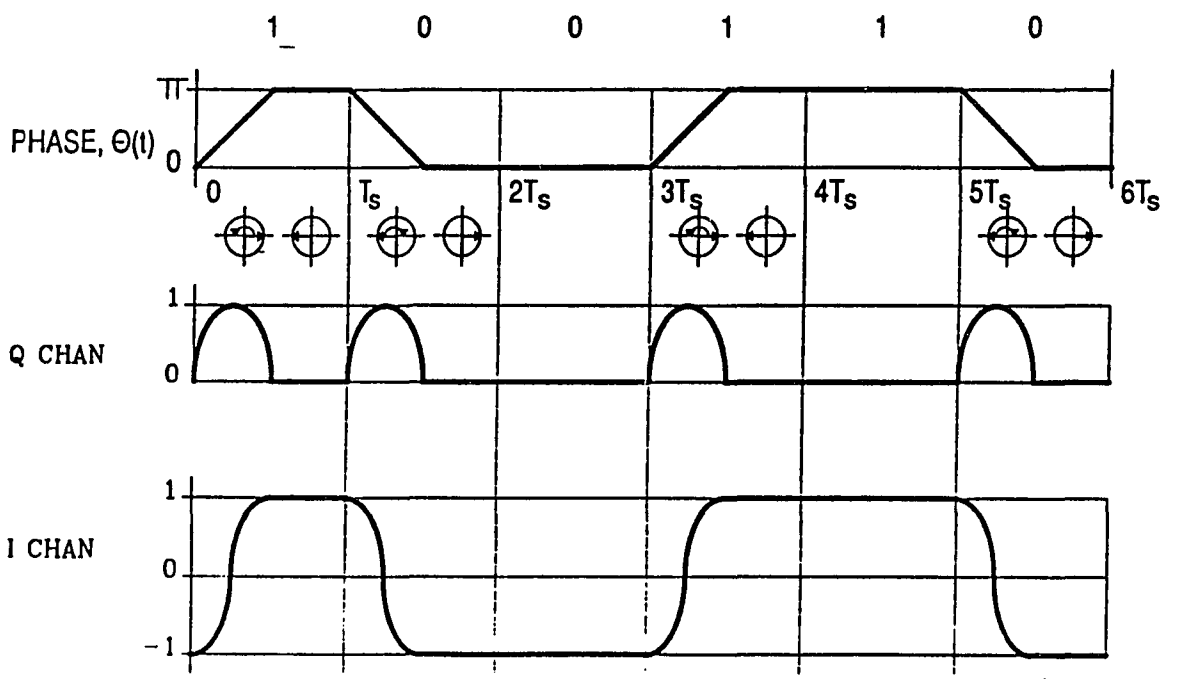

Figure 1.4: JCS SBPSK Modulation Format

Dapper and Hill 50% SBPSK

- o Existing "improvement" of JCS SBPSK .
- o I channel same as JCS SBPSK
- o Q channel average power is same as JCS SBPSK
- o Q channel average scalar is zero

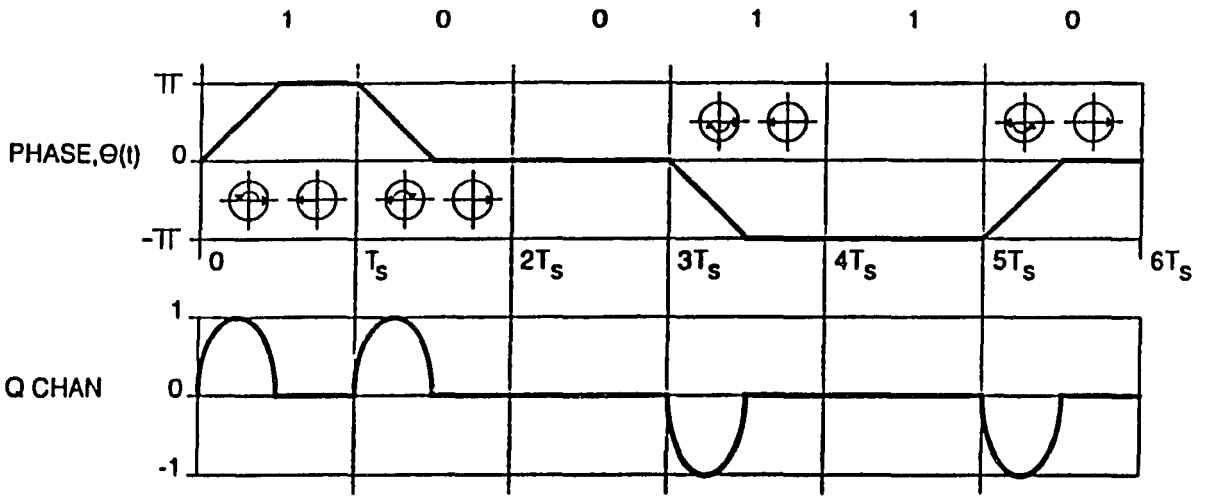

Figure 1.5: 50% Dapper and Hill SBPSK Modulation Format

"complex plane" (where the imaginary axis is the Q channel signal and the real axis is the I channel signal.) This rotation description still prevents net carrier frequency offset, and in addition prevents Q channel offset as well.

2. Whereas JCS SBPSK is specified to contain phase transitions over 50 percent of a bit interval, D&H SBPSK allow the fraction of the bit interval over which phase rotations occur to be a parameter of the modulation. For example, 50% D&H SBPSK refers to Dapper and Hill SBPSK with phase transitions occurring over 50 percent of a bit interval. In this respect 50% D&H SBPSK is analogous to JCS SBPSK; both are characterized by phase rotations occurring over 50 percent of a bit interval when that bit is of opposite polarity of the previous bit.

Figure 1.5 illustrates the phase rotations of 50% D&H SBPSK and the corresponding in-phase and quadrature channel signals.

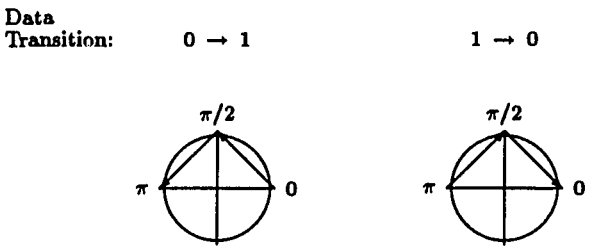

Figure 1.6: Modulation format for Modified BPSK by Yazdani et al.

From figures 1.4 and 1.5 it is seen that the phase vector always has a constant magnitude; it traces either a semicircle (JCS SBPSK) or a circle (D&H SBPSK) on the complex plane. It is this attribute that is responsible for the constant amplitude envelope of these modulations. If classical BPSK were postmodulation-filtered to obtain some desired bandlimited property, the result would be a phase vector that would remain on the real axis of the complex plain. The bandlimiting would be accomplished by "shrinking" the phase vector in magnitude when a phase transition occurs. This results in a signal with a high AM characteristic. As mentioned earlier, AM is forbidden by the JCS specification because the hardlimiting channel will remove the AM characteristic and thus the postmodulation filtering that was performed.

It is worthwhile to also note that Yazdani *et al.* propose a nearly constant amplitude envelope "Modified BPSK" in [3]. This modulation is characterized by a phase vector whose tip traces *arcs* rather than semicircles on the complex plane. When a data transition occurs the phase vector traces an arc from the real axis to the imaginary axis and then another arc back down to a point on the real axis directly opposite the point from which the phase transition began. See Figure 1.6. Because the magnitude of the phase vector is not constant, neither is the envelope of the amplitude of the modulated signal. Thus, this modulation is intermediate between that of classical BPSK and the SBPSK's of JCS and D&H. Its amplitude envelope is not constant, but it does not contain the degree of AM that classical BPSK would if postmodulation-filtered to obtain comparable spectral characteristics.

This thesis will present a new Shaped BPSK similar to that proposed by Dapper and Hill. Whereas Dapper and Hill specify constant rate phase rotations, a generalized SBPSK family will be presented in which the rate of change of phase may be specified by an arbitrary pulse shape that satisfies certain criteria. This new modulation will be described vigorously and compared with BPSK, JCS SBPSK, and D&H SBPSK in following chapters.

1.3 Research Objectives

As discussed in the previous section, there are a number of proposed BPSK interoperable modulation formats that obtain good spectral containment compared with classical BPSK and are characterized by constant amplitude envelopes. This study will propose a new, general family of modulations and compare the performance of a few members to the existing SBPSK formats and to classical BPSK.

Chapter 2 contains a mathematical description of the family of BPSK interoperable modulation formats presented here. The new modulation description is compared with existing modulation descriptions to elucidate similarities and differences with respect to existing modulations. Sample time-domain waveforms are presented for various SBPSK modulations that will be investigated in Chapters 3,4 and 5.

Chapter 3 investigates the spectral properties of the modulations discussed in previous chapters. Power spectral densities and fractional out-of-band power curves reveal that significant spectral containment can be achieved using shaped modulations. It is also shown that certain modulations are appropriate for use with the 5 kHz SATCOM channels described previously.

Chapter 4 presents an analysis of the signals discussed. This analysis includes equivalent SNR curves and probability of error curves. Although the use of SBPSK modulations increases spectral containment and reduces ACI, it is provided at the expense of the I channel energy required for demodulation. Equivalent SNR curves are presented to measure these effects. Finally, probability

of error curves are supplied to demonstrate the effects of a bandlimited, hardlimited channel on the different modulations presented.

Chapter 5 presents conclusions drawn from the study and suggests possible areas for further investigation.

CHAPTER 2

Shaped BPSK: A Class of BPSK/CPM Hybrid Modulations

This chapter will define a general Shaped BPSK (SBPSK) modulation format. The modulations are BPSK interoperable and have both continuous phase and constant amplitude envelopes. For these reasons, SBPSK may be thought of as a class of BPSK/CPM hybrid modulations.

In an effort to understand the characteristics of these modulations, they will be derived as special cases of the larger class of constant amplitude signals. First, a general expression for constant amplitude signals will be presented. Next, BPSK and CPM will be defined as special cases of the constant amplitude signals. The restrictions that are placed upon the general expression to obtain BPSK and CPM will be analyzed. It is then evident what characteristics are required to obtain BPSK/CPM hybrid modulations. It is also clear how these modulations are similar and how they differ. Finally, mathematical expressions for JCS SBPSK, D&H SBPSK, and the generalized version of D&H SBPSK will be presented as specific BPSK/CPM hybrid modulations. Chapter 2 will conclude with the presentation of sample waveforms for various SBPSK modulations.

2.1 Constant Amplitude Signals

An extremely general set of constant amplitude envelope signals can be defined by:

$$s(t) = \sqrt{2E/T}\cos(\omega_c t + \phi(t,\alpha)) \tag{2.1}$$

where

$$\phi(t,\alpha) = 2\pi h \sum_{i=-\infty}^{\infty} \alpha_i q(t - iT). \tag{2.2}$$

The parameter h is referred to as the modulation index. E is the energy per symbol, ω_c is the carrier frequency, and T is the symbol time. The transmitted symbols, α_i, determine the magnitude and polarity of signal phase changes. The function $q(t)$ is the signal phase response and may be expressed as:

$$q(t) = \int_{-\infty}^{t} g(\tau)\, d\tau.$$

The pulse shape $g(t)$ determines the rate of change of phase and is normalized so that it integrates to 1/2. Thus, $q(\infty) = 1/2$. At present there are no restrictions on the values of α_i or the shapes $g(t)$ and $q(t)$.

Virtually all constant amplitude envelope signals are special cases of (2.1) including BPSK, CPM, and BPSK/CPM hybrids. BPSK/CPM hybrids form a large class of SBPSK modulations and include JCS SBPSK, D&H SBPSK, and a generalized version of D&H SBPSK to be presented. The remaining sections of this chapter will demonstrate how each of the above modulations is obtained from equation (2.1). During these discussions, it will be helpful to refer to Table 2.1 located on page 31. This table summarizes the restrictions placed on equation (2.1) to obtain each modulation discussed.

2.2 BPSK

Binary Phase Shift Keying (BPSK) is the lowest order modulation of the general class of phase modulated signals called M-PSK. M denotes the modulation order and represents the number of different symbols contained in the symbol set. All transmitted symbols must be members of the symbol set. The higher the modulation order M, the greater the number of symbols in the symbol set, and hence the more *information* each symbol conveys. In the absence of channel noise, $\log_2 M$ expresses the number of bits of information each transmitted symbol represents. Thus 2-PSK, better known as BPSK, is a modulation format in which transmitted symbols are selected from of a set of

two symbols. Each transmitted symbol represents only one bit of information. A BPSK signal is most simply expressed as

$$s(t) = \sum_{i=-\infty}^{\infty} a_i p(t - iT) \sqrt{2E/T} \cos(\omega_c t). \tag{2.3}$$

The a_i are the binary data symbols and take the values $+1$ and -1. E is the energy per symbol, T is the symbol time, and ω_c is the carrier frequency. The pulse $p(t) = \text{rect}(\frac{t-T/2}{T})$.

BPSK may equivalently be expressed as

$$s(t) = \sqrt{2E/T} \cos(\omega_c t + \phi(t, a)) \tag{2.4}$$

where

$$\phi(t, a) = \pi/2 - \pi/2 \sum_{i=-\infty}^{\infty} a_i p(t - iT). \tag{2.5}$$

This form emphasizes the fact that BPSK has a constant amplitude envelope since the amplitude of the radio frequency cosine wave is always $\sqrt{2E/T}$. It is also easily seen that the transmitted information resides in the signal phase. The phase $\phi(t, a)$ is zero radians when $a_i = +1$ and π radians when $a_i = -1$. Clearly, $\phi(t, a)$ exhibits 180 degree phase changes whenever transitions in the binary data stream occur.

A third representation of BPSK is given by

$$s(t) = \sqrt{2E/T} \cos(\omega_c t + \phi(t, \alpha)) \tag{2.6}$$

where

$$\phi(t, \alpha) = 2\pi h \sum_{i=-\infty}^{\infty} \alpha_i q(t - iT). \tag{2.7}$$

The phase response $q(t) = \frac{1}{2}u(t)$ where $u(t)$ is the unit step function. The modulation index $h = 1$. The transmitted symbols α_i are members of the set $\{-1, 0, +1\}$. The symbol sequence $\{\alpha_i\}_{i=-\infty}^{\infty}$ is derived from the data bit sequence $\{a_i\}_{i=-\infty}^{\infty}$ by a mapping $U : \{a_i\}_{i=-\infty}^{\infty} \rightarrow \{\alpha_i\}_{i=-\infty}^{\infty}$. U is any

mapping that isolates transitions in the input data sequence and maps them to $\alpha_i = +1$ or -1. In other words,

$$U : \{a_i\}_{i=-\infty}^{\infty} \rightarrow \{\alpha_i\}_{i=-\infty}^{\infty} \text{ such that } \alpha_i = \begin{cases} +1 \text{ or } -1 & \text{if } a_i \neq a_{i-1} \\ 0 & \text{if } a_i = a_{i-1}. \end{cases} \tag{2.8}$$

For example, the equation $\alpha_i = a_i - a_{i-1}$ is a valid mapping.

Examination of the set $\{\alpha_i\}$, the phase response $q(t)$, and the modulation index, h, reveals that the signal phase $\phi(t, \alpha)$ will always remain stationary when $\alpha_i = 0$, instantaneously advance π radians when $\alpha_i = 1$, or equivalently, retard π radians when $\alpha_i = -1$. Selection of a mapping, U, that satisfies the criteria above insures that $\phi(t, \alpha)$ will exhibit 180 degree phase changes whenever transitions in the binary data occur.

Although this representation is not as straightforward as that of (2.3), it does show that BPSK is a special case of the constant amplitude envelope signals. It is obtained by placing restrictions on three elements of equation (2.1). These restrictions are:

1. The transmitted symbols α_i take values $-1, 0$, and $+1$. This results in a transmitted signal whose phase during symbol i may advance, retard or remain stationary relative to the signal phase during symbol $i - 1$. In addition a mapping U must be provided to map binary data bits to ternary transmitted symbols. U must satisfy equation (2.8).

2. The pulse shape $g(t) = \frac{1}{2}\delta(t)$ results in phase shifts that occur instantaneously when the signal phase advances or retards.

3. The modulation index $h = 1$ forces the magnitude of phase changes to be 180 degrees.

This is summarized in Table 2.1 on page 31.

2.3 CPM

Continuous Phase Modulation (CPM) refers to a large class of constant amplitude envelope signals with continuous phase. These signals are defined by Sundberg in [4] as

$$s(t) = \sqrt{2E/T}\cos(\omega_c t + \phi(t, \alpha)) \tag{2.9}$$

where the transmitted information is contained in the phase

$$\phi(t, \alpha) = 2\pi h \sum_{i=-\infty}^{\infty} \alpha_i q(t - iT) \tag{2.10}$$

with $q(t) = \int_{-\infty}^{t} g(\tau)\, d\tau$. The pulse shape $g(t)$ is of finite duration; it is zero outside the interval $0 \leq t \leq LT$. L represents the length of $g(t)$ in units of symbol time, T. E is the energy per symbol, ω_c is the carrier frequency, and h is the modulation index. The M-ary transmitted symbols are elements of the set $\{-(M-1), \ldots, -3, -1, +1, +3, \ldots, +(M-1)\}$ with M typically a power of two.

The pulse $g(t)$ is defined in instantaneous frequency, and its integral $q(t)$ is the phase response. The shape of $g(t)$ determines the smoothness of the information carrying phase. To maintain continuous phase, $g(t)$ must never contain impulses. This implies that the phase $q(t)$ will never contain "steps," or discontinuities.

Comparison of equation (2.9) with equation (2.1) shows that CPM is also a special case of the constant amplitude envelope signals. For CPM, restrictions are placed on two elements of equation (2.1):

1. To maintain continuous phase the pulse shape $g(t)$ must not contain any impulses.

2. The transmitted symbols α_i are members of the set $\{-(M-1), \ldots, -3, -1, +1, +3, \ldots, +(M-1)\}$ which results in a signal phase that *always* advances or retards for every symbol transmitted.

2.4 BPSK/CPM Hybrid Modulations

CPM signals are known to exhibit excellent spectral properties [4] –[10]. In an effort to impart some of this spectral efficiency to BPSK signaling, hybrid modulations have been proposed. BPSK/CPM hybrid modulations are essentially BPSK signals with the instantaneous 180 degree phase transitions replaced with phase rotations occurring over some fraction of the symbol period. They are referred to as Shaped BPSK (SBPSK) modulations. JCS SBPSK, Dapper and Hill SBPSK, and a generalized version of D&H SBPSK all are BPSK/CPM hybrids.

In the previous two sections, BPSK and CPM were independently defined in terms of equation (2.1). Restrictions on certain elements of the equation were necessary to obtain BPSK and CPM as special cases of the constant amplitude signals. For BPSK, the modulation index equals one, the pulse shape $g(t)$ is an impulse, and the transmitted symbols are obtained from the binary data by the mapping U. For CPM, the modulation index is arbitrary, the pulse shape $g(t)$ does not contain impulses and is of finite duration, and the transmitted symbol set does not contain the element zero. In order to obtain a modulation that exhibits 180 degree continuous phase rotations over some portion of a bit interval when data transitions occur, the following conditions must be satisfied:

1. The modulation index, h, must equal one,

2. A mapping U that satisfies (2.8) must be provided, and

3. The pulse shape $g(t)$ must not contain impulses. To insure that phase rotations are confined to one symbol period, $g(t)$ must be zero outside the interval $0 \leq t \leq T$. Of course $g(t)$ is still normalized so that it integrates to 1/2.

This list provides the restrictions on equation (2.1) that yield BPSK/CPM hybrid modulations. JCS SBPSK, D&H SBPSK, and a generalized D&H SBPSK are presented in the following subsections.

2.4.1 JCS SBPSK

In Section 1.2, JCS SBPSK was presented qualitatively. The modulation was described as having constant-rate phase rotations when transitions occur in the transmitted data stream. The current rotation is always in the opposite direction of the preceding rotation so that net carrier frequency offset is avoided.

JCS SBPSK, like the modulations in previous sections, is a special case of equation (2.1). For JCS SBPSK the restricted elements of (2.1) are

1. The modulation index $h = 1$,
2. The mapping $U_{\text{JCS SBPSK}}$ is defined by $\alpha_i = a_i - a_{i-1}$, and
3. The pulse shape $g(t) = \frac{1}{T}\text{rect}(\frac{t-T/4}{T/2})$.

The pulse shape $g(t)$ represents the rate of change of signal phase when transitions occur. Clearly the phase rotations are "constant-rate." The phase response $q(t)$ is simply a ramp function:

$$q(t) = \begin{cases} 0 & \text{for } t < 0 \\ t/T & \text{for } 0 \leq t \leq T/2 \\ 1/2 & \text{for } t > T/2. \end{cases}$$

It is apparent that the signal phase response is continuous.

2.4.2 Dapper and Hill SBPSK

In Section 1.2, Dapper and Hill SBPSK was described qualitatively. Like JCS SBPSK, this modulation is described as having constant-rate phase rotations when transitions occur in the binary data stream. Unlike JCS SBPSK, D&H SBPSK comprises an entire family of modulations. Members are indexed by the fraction of a symbol interval, λ, over which phase rotations occur. Also, the direction of phase rotation is not always opposite that of the previous rotation. Instead the phase rotates in the same direction twice after which the following two rotations will be in the opposite direction.

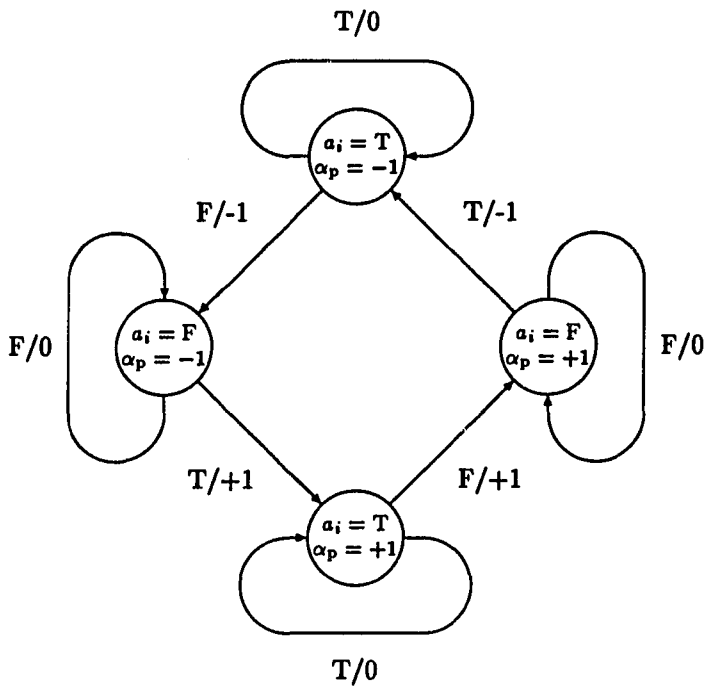

In this diagram, the input data a_i is expressed as T and F instead of +1 and -1.

The notation a_i/α_i implies that the input a_i maps to the output α_i.

Each state is determined by the input data a_i and α_p, the last (or *previous*) non-zero α_i.

Figure 2.1: State Diagram for $U_{\text{D\&H SBPSK}}$

Dapper and Hill SBPSK is obtained from equation (2.1) when

1. $h = 1$,
2. the mapping $U_{\text{D\&H SBPSK}}$ is defined by the state diagram presented in Figure 2.1, and
3. the pulse shape $g(t) = \frac{1}{2\lambda T}\text{rect}(\frac{t-\lambda T/2}{\lambda T})$ where λ is the fraction of the symbol interval over which phase rotations occur.

From Figure 2.1 it can be seen that a change of state occurs only when the data bit a_i is different than the previous bit a_{i-1}. A change of state is always accompanied by $\alpha_i = -1$ or $+1$. Thus, $U_{\text{D\&H SBPSK}}$ satisfies equation (2.8).

2.4.3 Generalized Dapper and Hill SBPSK

Dapper and Hill SBPSK has many fine qualities. The arbitrary length of $g(t)$ conveniently defines an entire family of modulations. The design of $U_{\text{D\&H SBPSK}}$ prevents both net carrier frequency offset and average Q channel offset. It will be seen in Chapter 3 that this mapping also results in desirable spectral properties. The only shortcoming of D&H SBPSK is the unnecessary restriction of constant-rate phase rotations. By redefining $g(t)$ to be any impulse-free pulse shape, generalized D&H SBPSK results. These modulations are obtained from equation (2.1) when

1. $h = 1$,

2. a_i are mapped to α_i by $U_{\text{D\&H SBPSK}}$, and

3. the pulse shape $g(t)$ is any impulse-free pulse shape that integrates to 1/2.

We adopt the following shorthand notation to represent specific "generalized D&H SBPSK" modulations. The duration of $g(t)$ is expressed as a percent of the symbol interval and is followed by the name of the pulse shape. For example, *25% Hamming SBPSK* refers to a generalized D&H SBPSK modulation in which $g(t)$ is a Hamming pulse of duration $\frac{1}{4}T$. Table 2.2 presents a summary of the pulse shapes for specific "generalized D&H SBPSK" modulations. The pulse shape definitions were obtained from Harris [11].

2.5 Examples of SBPSK Waveforms

In previous sections, constant amplitude signals were expressed as $s(t) = \sqrt{2E/T}\cos(\omega_c t + \phi(t,\alpha))$ where $\phi(t,\alpha) = 2\pi h \sum_{i=-\infty}^{\infty} \alpha_i q(t-iT)$. For BPSK and SBPSK modulations, $h = 1$ and U maps a_i to α_i. The phase response $q(t) = \int_{-\infty}^{t} g(\tau)\,d\tau$ where the pulse shape $g(t)$ determines the rate of change of the signal phase.

Examples of BPSK and SBPSK signals are provided in the figures below. For each modulation, a set of sample waveforms is presented. Each set contains the following waveforms:

1. the pulse shape $g(t)$,
2. the transmitted data $\bar{a}_i$,
3. the rate of change of the signal phase $\frac{d\phi(t,\alpha)}{dt}$,
4. the signal phase $\phi(t,\alpha)$,
5. the bandpass signal $s(t)$ when $2\pi\omega_c = \frac{2}{T}$,
6. the in-phase (I channel) signal, and
7. the quadrature (Q channel) signal.

While viewing these examples, note that the amount of energy in the I and Q channels differs from modulation to modulation. The ramifications of this are the subject of much of Chapter 4.

	BPSK	CPM	SBPSK: BPSK/CPM Hybrid Modulations			
			General SBPSK Requirements	Specific SBPSK Modulations		
				JCS SBPSK	D&H SBPSK	Generalized D&H SBPSK
modulation index, h	1	arbitrary	1	1	1	1
U_{MAP}	satisfies equation (2.8)	U_{CPM}[a]	satisfies equation (2.8)	$U_{\text{JCS SBPSK}}$	$U_{\text{D\&H SBPSK}}$	$U_{\text{D\&H SBPSK}}$
$g(t)$	$\frac{1}{2}\delta(t)$	no impulses	no impulses	$\frac{1}{T}\text{rect}(\frac{t-T/4}{T/2})$	$\frac{1}{2\lambda T}\text{rect}(\frac{t-\lambda T/2}{\lambda T})$	no impulses

[a] U_{CPM} is not like the other mappings. The other mappings encode one binary digit (bit) into one ternary symbol. These are *pseudoternary codes* since each of the ternary symbols still conveys only one bit of information. U_{CPM} maps $\log_2 M$ bits into one of M transmitted symbols. Thus, each M-ary symbol represents $\log_2 M$ bits. The only meaningful comparison is for Binary CPM, in which case, U_{BCPM} would be trivial, $\alpha_i = a_i$.

Table 2.1: Parameters for Selected Constant Amplitude Signals

MODULATION	PULSE SHAPE
$x\%$ Hamming SBPSK	$g(t) = \begin{cases} \frac{0.926}{T\lambda}[0.54 - 0.46\cos(\frac{2\pi}{T\lambda}t)] & 0 \le t \le T\lambda \\ 0 & \text{elsewhere} \end{cases}$
$x\%$ Min. 3 Term Blackman SBPSK	$g(t) = \begin{cases} \frac{1.19}{T\lambda}[0.42323 - 0.49755\cos(\frac{2\pi}{T\lambda}t) + 0.07922\cos(\frac{4\pi}{T\lambda}t)] & 0 \le t \le T\lambda \\ 0 & \text{elsewhere} \end{cases}$
$x\%$ Sin SBPSK	$g(t) = \begin{cases} \frac{\pi/4}{T\lambda}\sin(\frac{\pi t}{T\lambda}) & 0 \le t \le T\lambda \\ 0 & \text{elsewhere} \end{cases}$
$x\%$ Sin^2 SBPSK	$g(t) = \begin{cases} \frac{1}{T\lambda}\sin^2(\frac{\pi t}{T\lambda}) & 0 \le t \le T\lambda \\ 0 & \text{elsewhere} \end{cases}$
$x\%$ Sin^3 SBPSK	$g(t) = \begin{cases} \frac{1.20}{T\lambda}\sin^3(\frac{\pi t}{T\lambda}) & 0 \le t \le T\lambda \\ 0 & \text{elsewhere} \end{cases}$
$x\%$ Tukey 25% Rolloff SBPSK	$g(t) = \begin{cases} \frac{0.568}{T\lambda} \cdot \begin{cases} 1 & 0 \le \lvert t - \frac{T\lambda}{2} \rvert \le 0.75\frac{T\lambda}{2} \\ \frac{1}{2}[1 + \cos(\pi\frac{\lvert t - \frac{T\lambda}{2}\rvert - 0.75\frac{T\lambda}{2}}{0.25\frac{T\lambda}{2}})] & 0.75\frac{T\lambda}{2} \le \lvert t - \frac{T\lambda}{2} \rvert \le \frac{T\lambda}{2} \end{cases} & 0 \le t \le T\lambda \\ 0 & \text{elsewhere} \end{cases}$
$x\%$ Tukey 50% Rolloff SBPSK	$g(t) = \begin{cases} \frac{0.667}{T\lambda} \cdot \begin{cases} 1 & 0 \le \lvert t - \frac{T\lambda}{2} \rvert \le 0.50\frac{T\lambda}{2} \\ \frac{1}{2}[1 + \cos(\pi\frac{\lvert t - \frac{T\lambda}{2}\rvert - 0.50\frac{T\lambda}{2}}{0.50\frac{T\lambda}{2}})] & 0.50\frac{T\lambda}{2} \le \lvert t - \frac{T\lambda}{2} \rvert \le \frac{T\lambda}{2} \end{cases} & 0 \le t \le T\lambda \\ 0 & \text{elsewhere} \end{cases}$
$x\%$ Tukey 75% Rolloff SBPSK	$g(t) = \begin{cases} \frac{0.794}{T\lambda} \cdot \begin{cases} 1 & 0 \le \lvert t - \frac{T\lambda}{2} \rvert \le 0.25\frac{T\lambda}{2} \\ \frac{1}{2}[1 + \cos(\pi\frac{\lvert t - \frac{T\lambda}{2}\rvert - 0.25\frac{T\lambda}{2}}{0.75\frac{T\lambda}{2}})] & 0.25\frac{T\lambda}{2} \le \lvert t - \frac{T\lambda}{2} \rvert \le \frac{T\lambda}{2} \end{cases} & 0 \le t \le T\lambda \\ 0 & \text{elsewhere} \end{cases}$

The variable λ represents the duration of $g(t)$ in terms of the symbol time T. $x\% = \lambda \cdot 100\%$.

Table 2.2: Pulse Shapes for Selected Generalized D&H Modulations

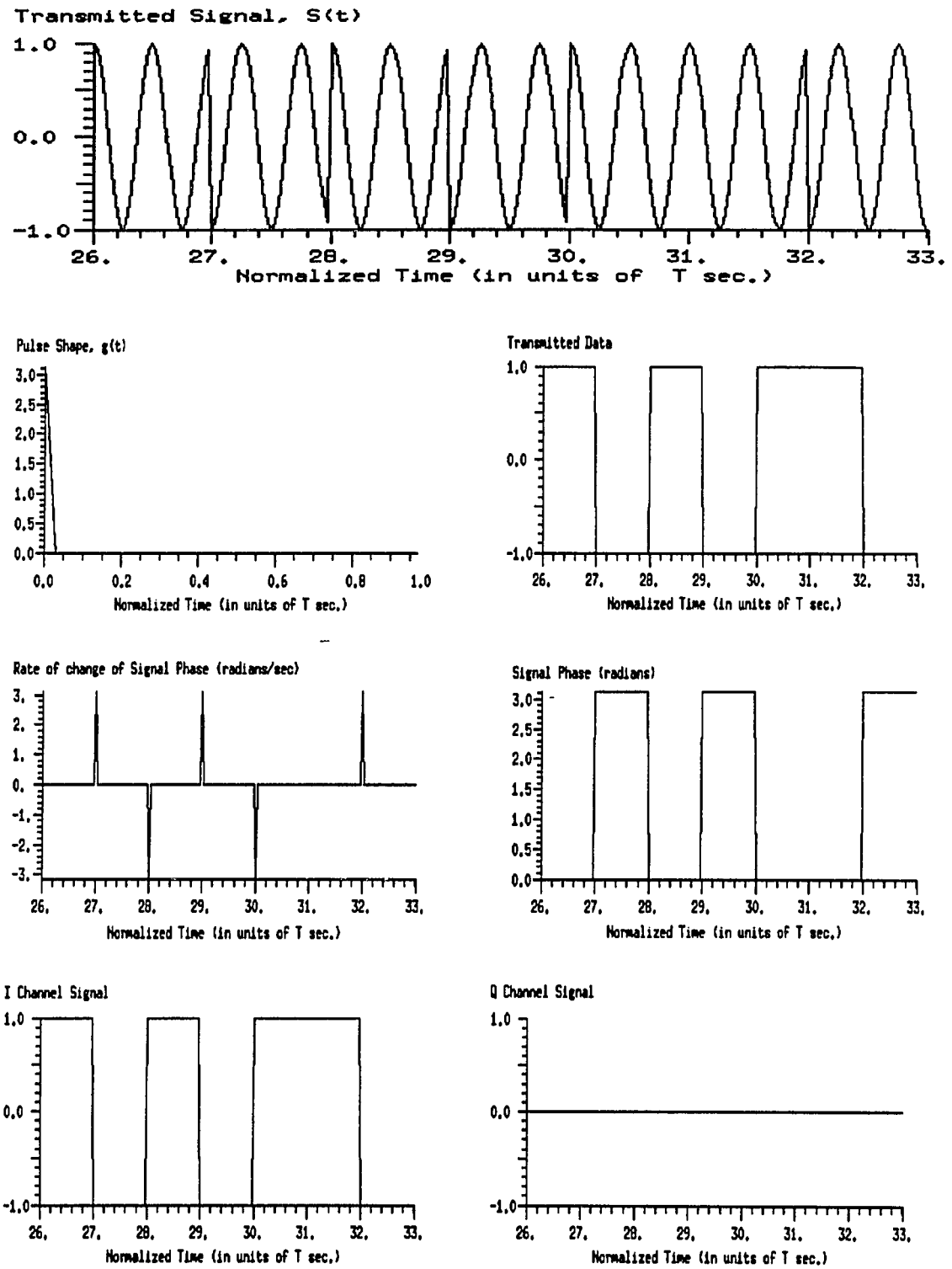

Figure 2.2: BPSK Sample Waveforms.

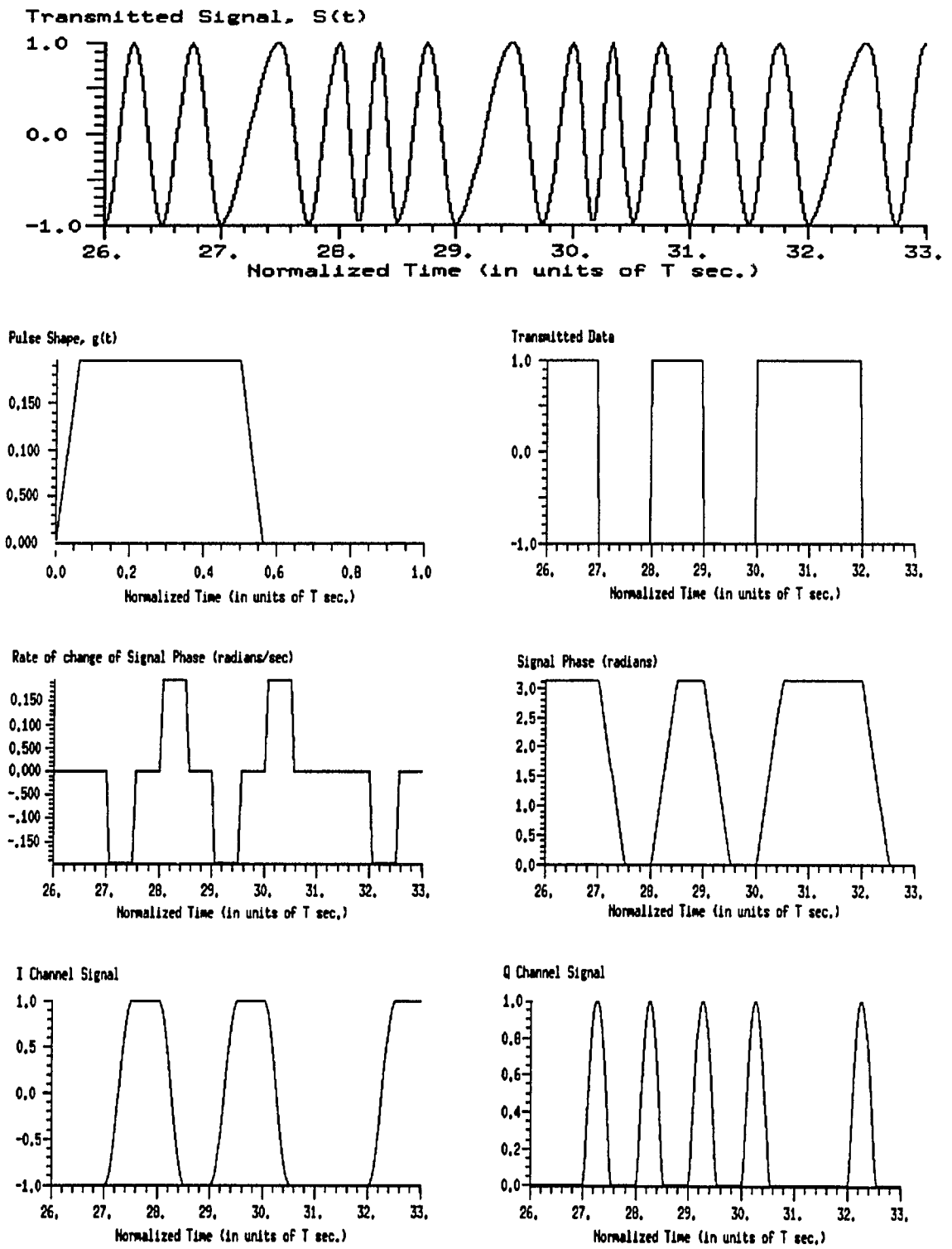

Figure 2.3: JCS SBPSK Sample Waveforms.

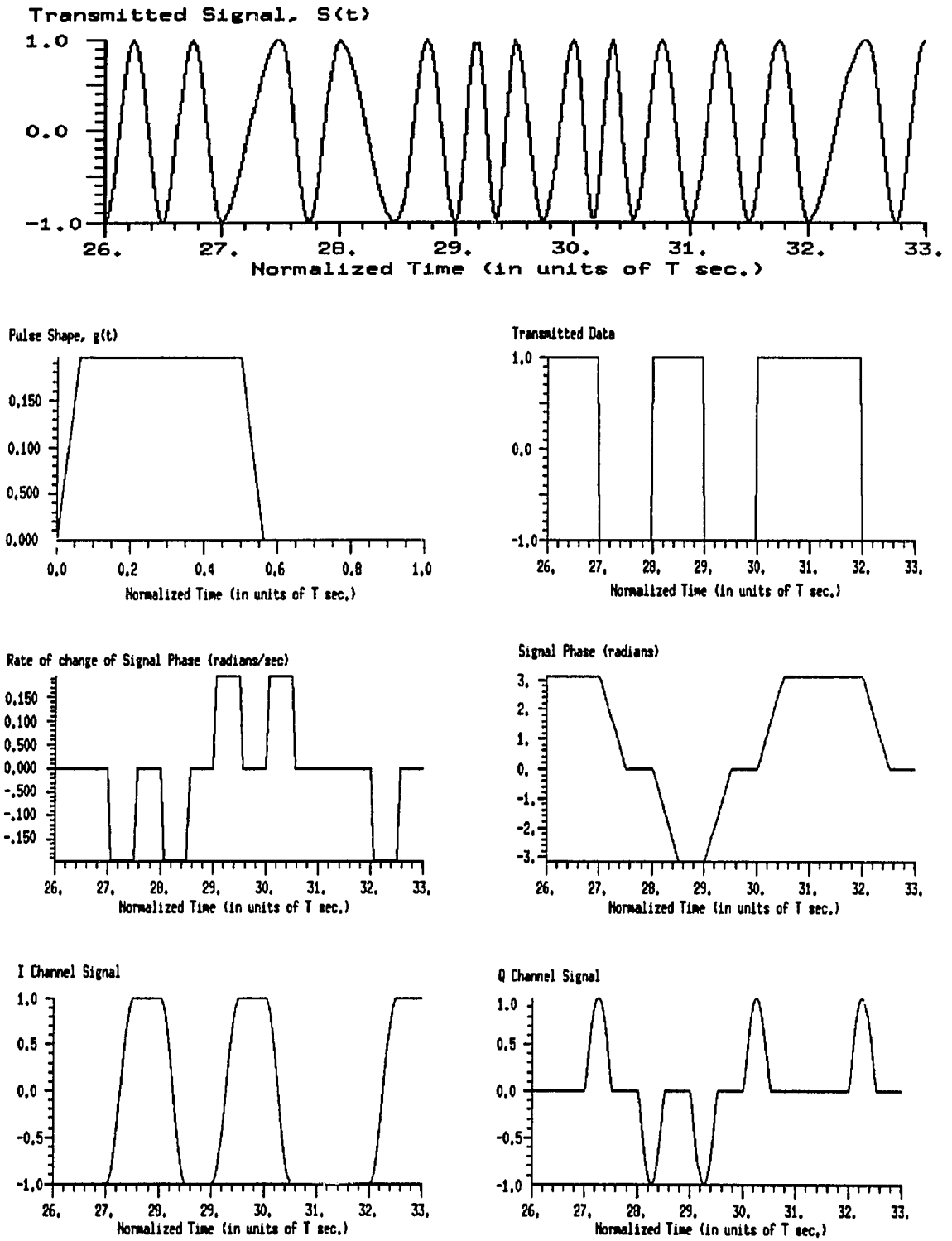

Figure 2.4: 50% Dapper and Hill SBPSK Sample Waveforms.

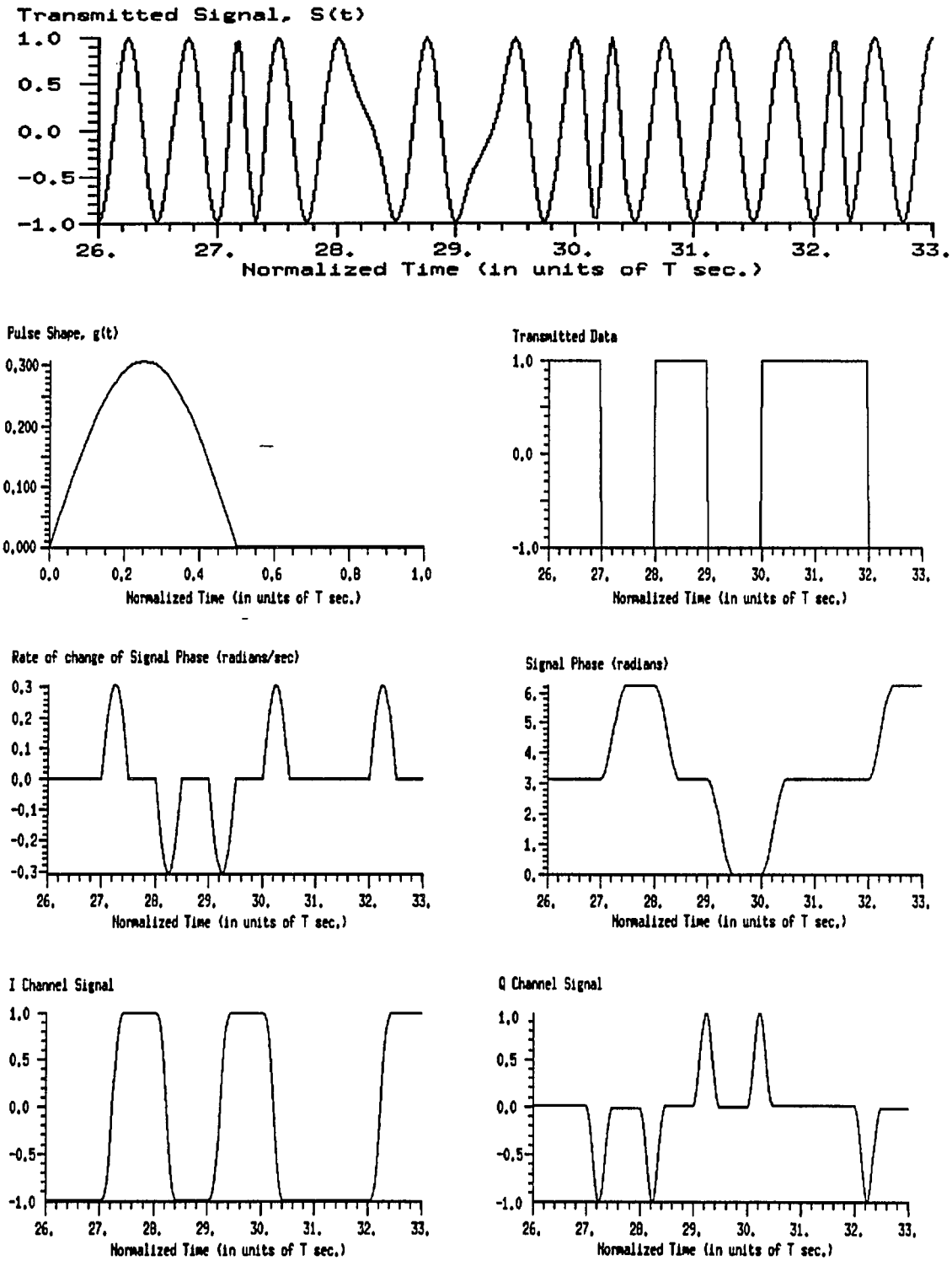

Figure 2.5: 50% Sin SBPSK Sample Waveforms.

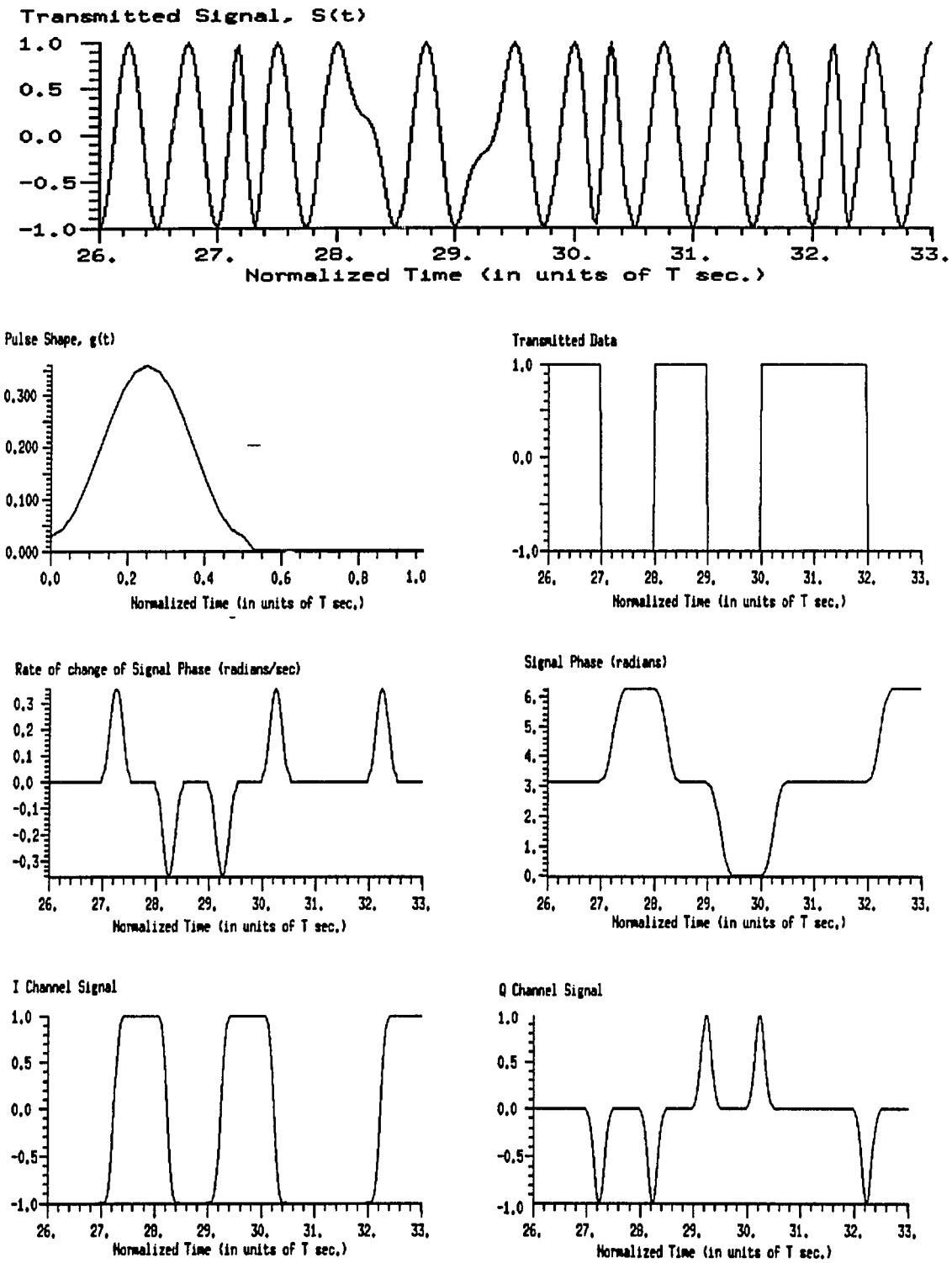

Figure 2.6: 50% Hamming SBPSK Sample Waveforms.

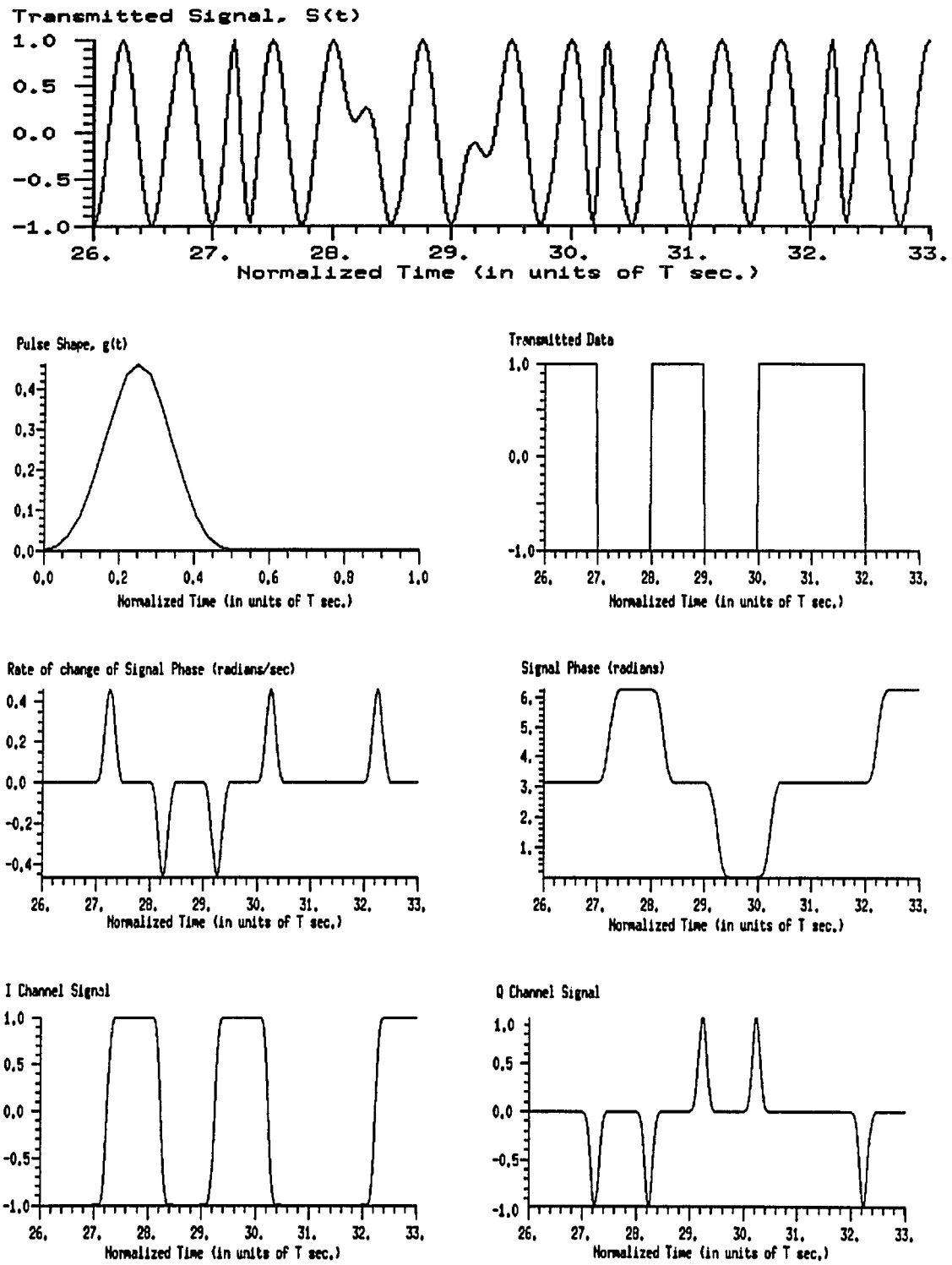

Figure 2.7: 50% Min. 3 Term Blackman SBPSK Sample Waveforms.

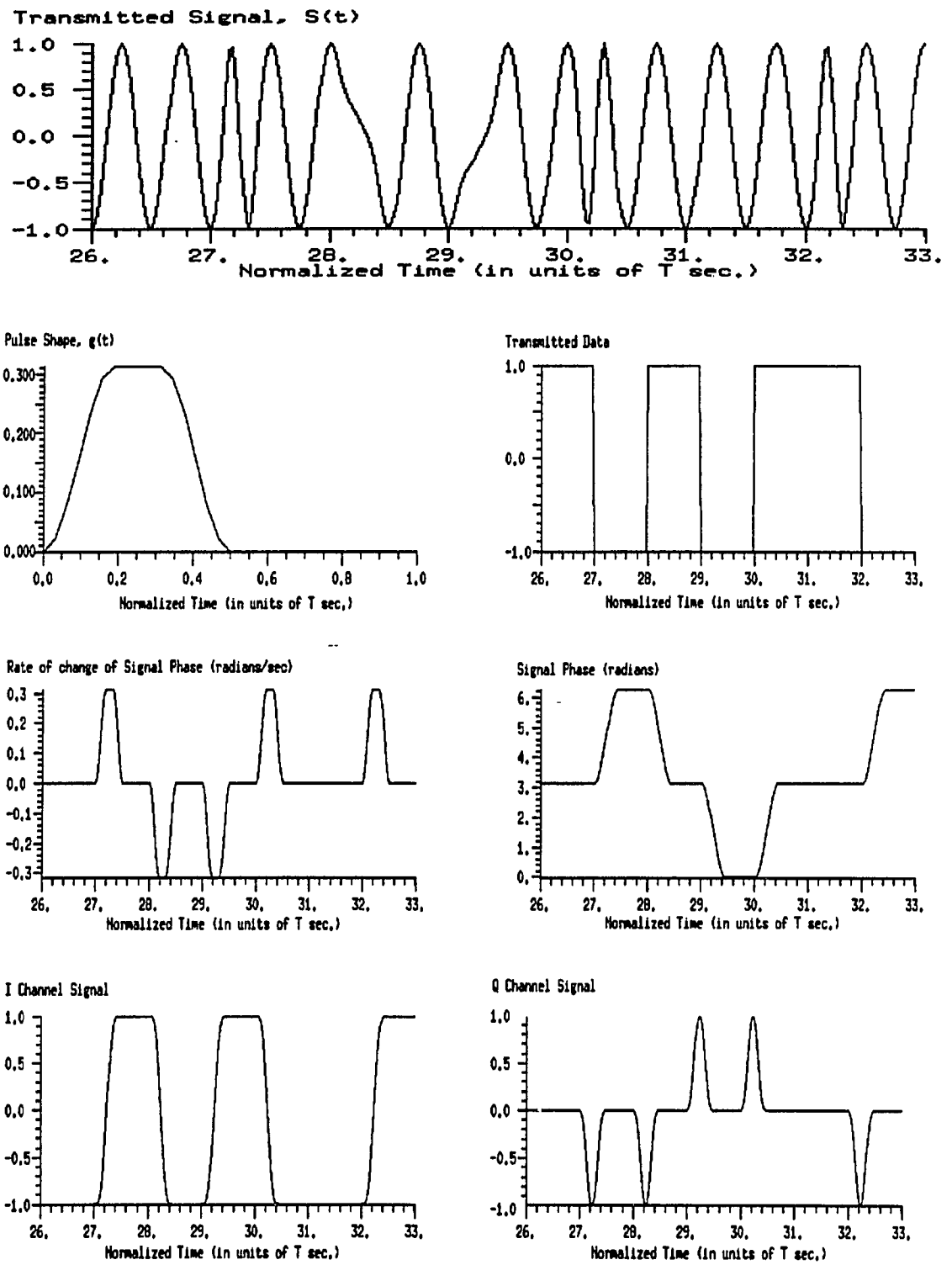

Figure 2.8: 50% Tukey 75% Rolloff SBPSK Sample Waveforms.

CHAPTER 3

Spectral Characteristics of SBPSK Signals

The frequency content of a signal is a basic characteristic that distinguishes one signal from another. In fact, this thesis is motivated by the desire to efficiently limit the frequency range of BPSK signals. The distribution of power as a function of frequency is known as the *power spectral density* or *power spectrum* of a signal. The first section of this chapter will introduce the statistical methods with which power spectral densities are obtained. The second section will present the psd's of the BPSK and SBPSK signals that were defined in Chapter 2. The final section of this chapter is devoted to "fractional out-of-band power curves."

3.1 Evaluation of Power Spectral Density

For wide-sense stationary stochastic processes with finite power, the power spectral density (psd) is the Fourier transform of the autocorrelation function. This is written as

$$S(f) = \int_{-\infty}^{\infty} \mathrm{R_S}(\tau)\, e^{-j2\pi f\tau}\, d\tau. \tag{3.1}$$

Three methods exist for obtaining the psd's of modulated signals such as BPSK and SBPSK. The first is to analytically solve equation (3.1). For BPSK with random initial phase this is possible. The well-known result is

$$S_{\mathrm{BPSK}}(f) \approx \frac{1}{2}\left[\frac{E\sin^2(\pi T(f-f_c))}{(\pi T(f-f_c))^2} + \frac{E\sin^2(\pi T(f+f_c))}{(\pi T(f+f_c))^2}\right] \tag{3.2}$$

when $f_c \gg 1/T$. This simple solution exists because BPSK can be represented as amplitude modulation (see equation (2.3)). For SBPSK, CPM, and other phase modulations, a non-linear

transformation of the baseband signal occurs. These signals cannot, in general, be represented by a linear carrier modulation as BPSK can. In these circumstances, semi-analytic and simulation/experimental methods are used to obtain psd's.

With the semi-analytic approach, equation (3.1) is partially solved. Usually, the statistical characteristics of the transmitted sequence $\{\alpha_i\}_{i=-\infty}^{\infty}$ imbedded within the modulated signal $s(t)$ are obtained analytically. The spectral characteristics (psd's) of each member of the set of transmitted waveforms are solved by numerical methods. A composite solution then results. A great deal of work has been done in this area to simplify the expressions for specific modulations [12] –[31].

For the simulation/experimental method, the psd of a stochastic process is estimated by analyzing a discrete-time version of a sample function of the stochastic process. The discrete-time sample function may be obtained from computations (simulation) or from sampling an analog signal (experimentation.) The discrete Fourier transform (DFT) performed on a finite length of the discrete-time sample function can be used to provide an estimate of the psd. This estimate can be made quite accurate if the discrete Fourier transform is carefully used.

Consider a stochastic process $s(t)$ for which the power spectral density is desired. An arbitrary sample function of this process is denoted $s_i(t)$. A discrete-time version of this sample function is expressed as $\{s_i(nT_{\text{samp}})\}_{n=-\infty}^{\infty}$ where $\frac{1}{T_{\text{samp}}}$ is the sampling frequency. A finite length subsequence is $\{s_i(nT_{\text{samp}})\}_{n=0}^{N-1}$ where N is the number of sample points in the subsequence. N is referred to as the *record length* of a finite length sequence. The discrete Fourier transform of a finite length sequence h is defined as

$$H(k\Delta f_{\text{res}}) = \begin{cases} \sum_{n=0}^{N-1} h(nT_{\text{samp}}) e^{j(2\pi/N)(-nk)} & \text{for } k = 0, 1, \ldots, N-1 \\ 0 & \text{otherwise} \end{cases}$$

where $\Delta f_{\text{res}} = \frac{1}{NT_{\text{samp}}}$.

Consequently, the DFT of the sequence $\{s_i(nT_{\text{samp}})\}_{n=0}^{N-1}$ is

$$S_i(k\Delta f_{\text{res}}) = \begin{cases} \sum_{n=0}^{N-1} s_i(nT_{\text{samp}})e^{j(2\pi/N)(-nk)} & \text{for } k = 0, 1, \ldots, N-1 \\ 0 & \text{otherwise} \end{cases}$$

and $|S_i(k\Delta f_{\text{res}})|^2$ is an estimate of $S(f)$, the power spectral density of the stochastic process $s(t)$.

Several properties of the DFT are important. Unlike the Fourier transform, which yields a continuous power spectrum, the DFT produces a discrete spectrum. In fact, the DFT is a sampled version of the Fourier transform where the samples are Δf_{res} Hz apart. Δf_{res} is referred to as the *frequency resolution* of the DFT. For "good" resolution, $\Delta f_{\text{res}} = \frac{1}{NT_{\text{samp}}}$ should be small. The *frequency range* of the DFT is

$$\Delta f_{\text{range}} = N\Delta f_{\text{res}} = \frac{1}{T_{\text{samp}}} \quad \text{Hz.}$$

For a wide frequency range, $\frac{1}{T_{\text{samp}}}$ should be large. Thus, for good frequency resolution over a wide range of frequencies, N must be sufficiently large. In addition, N must also be large so that the statistical properties of the finite sequence approximate the statistical properties of the stochastic process. For example, in the case of modulated signals such as BPSK and SBPSK, the sequence representing the discrete-time sample function must be long enough to demonstrate the randomness of the data. Simply stated, the DFT must "look" at the sample function for many transmitted symbols. The duration of the finite sequence expressed in units of transmitted symbols is $\frac{NT_{\text{samp}}}{T}$ where T is the transmitted symbol time. For the random data simulator used here, little improvement was seen in psd's obtained for record lengths greater than 256 symbols. (See Figure 3.1.)

To summarize, the DFT of a finite-length discrete-time sample function $\{s_i(nT_{\text{samp}})\}_{n=0}^{N-1}$ may be used to approximate the power spectral density of the stochastic process $s(t)$. The sequence may be obtained by computer simulation of the signal $s_i(t)$ or from sampling an analog signal. The approximated psd may be made arbitrarily accurate when the sample rate and the record length

are large enough. For a desired frequency resolution (Δf_{res_o}) and frequency range (Δf_{range_o}), N and T_{samp} must meet the following criteria:

$$\begin{aligned} T_{samp} &\leq \frac{1}{\Delta f_{range_o}} \\ N &\geq \frac{1}{\Delta f_{res_o}} \cdot \frac{1}{T_{samp}} \end{aligned}$$

also

$$\frac{NT_{samp}}{T} \geq 256 \text{ transmitted symbols} \quad \rightarrow \quad N \geq \frac{256\,T}{T_{samp}}.$$

Figure 3.1 provides examples of BPSK power spectral densities obtained by computer simulation. It can be seen that no significant improvement is seen for record lengths in excess of 256 symbols. The exact psd of BPSK obtained from equation (3.2) is plotted for reference.

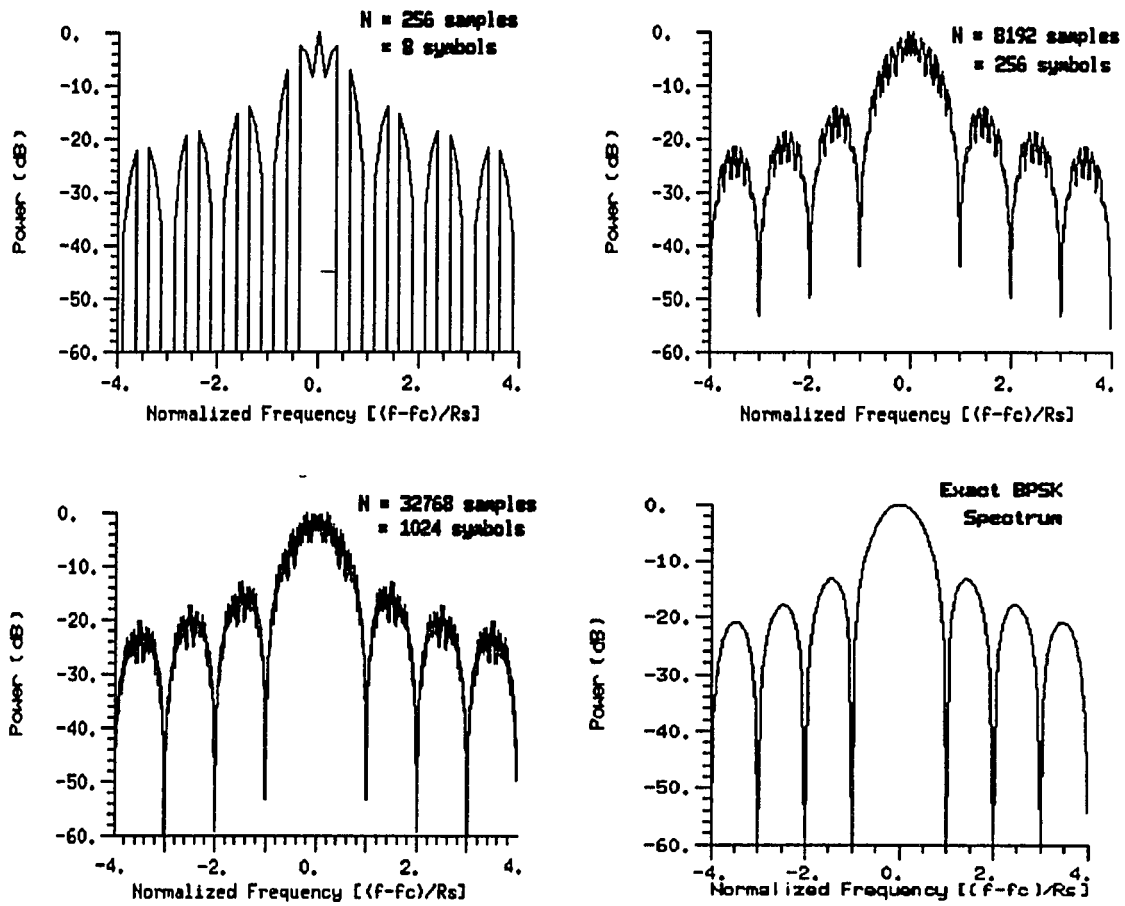

Figure 3.1: BPSK Power Spectral Densities via Computer Simulation.

3.2 Power Spectral Densities of SBPSK Modulations

In Chapter 2, various SBPSK signals were presented. The power spectral densities of these signals are provided in Figures 3.2 and 3.3. These psd's were obtained via computer simulation as described previously. For all modulations, the sampling frequency $\frac{1}{T_{samp}} = 32R_s$ where R_s is the transmitted symbol rate. The record length is 256 symbols. In both figures, the psd of BPSK appears as a reference.

Examination of these figures reveals an interesting, but not at all surprising, relationship between the spectral characteristics of the pulse shapes and the corresponding modulations. As the pulse shapes become "smoother", their spectrums exhibit increased mainlobe width and lower sidelobe height. This trend is incorporated into the psd's of the corresponding modulated signals. The power spectrums of the pulse shapes form "envelopes" on the psd's of the modulated signals. Consequently, we will refer to the mainlobe of the modulated signals as the range of frequencies contained in the mainlobe of the envelope induced upon the modulated signal psd's. For example, 50% Dapper and Hill SBPSK exhibits a mainlobe that encompasses 6 bit rates centered about f_c, while the mainlobe of 50% Hamming SBPSK is more than twice this width at 14 bit rates. Once outside the mainlobe, the benefits of lower sidelobes are revealed. At 7.5 bit rates from f_c, the psd of 50% Hamming SBPSK is 15 dB lower than that of 50% D&H SBPSK at the same frequency. It is important to note that the mainlobes of 50% D&H SBPSK and JCS SBPSK are the narrowest of the SBPSK signals. Clearly, this is due to the use of a square pulse whose mainlobe is the narrowest of the pulse shapes investigated here. As a result, the next section will reveal that these two modulations are the most spectrally efficient for narrowband channels.

Examination of these figures also shows that all modulations except JCS SBPSK exhibit spectral nulls at integer multiples of the symbol rate. This condition results when transmitted waveforms are symmetrically positioned in the complex plane [30]. BPSK satisfies this criteria since it is defined by the transmission of antipodal waveforms. As discussed in Section 2.2, the phase of a BPSK

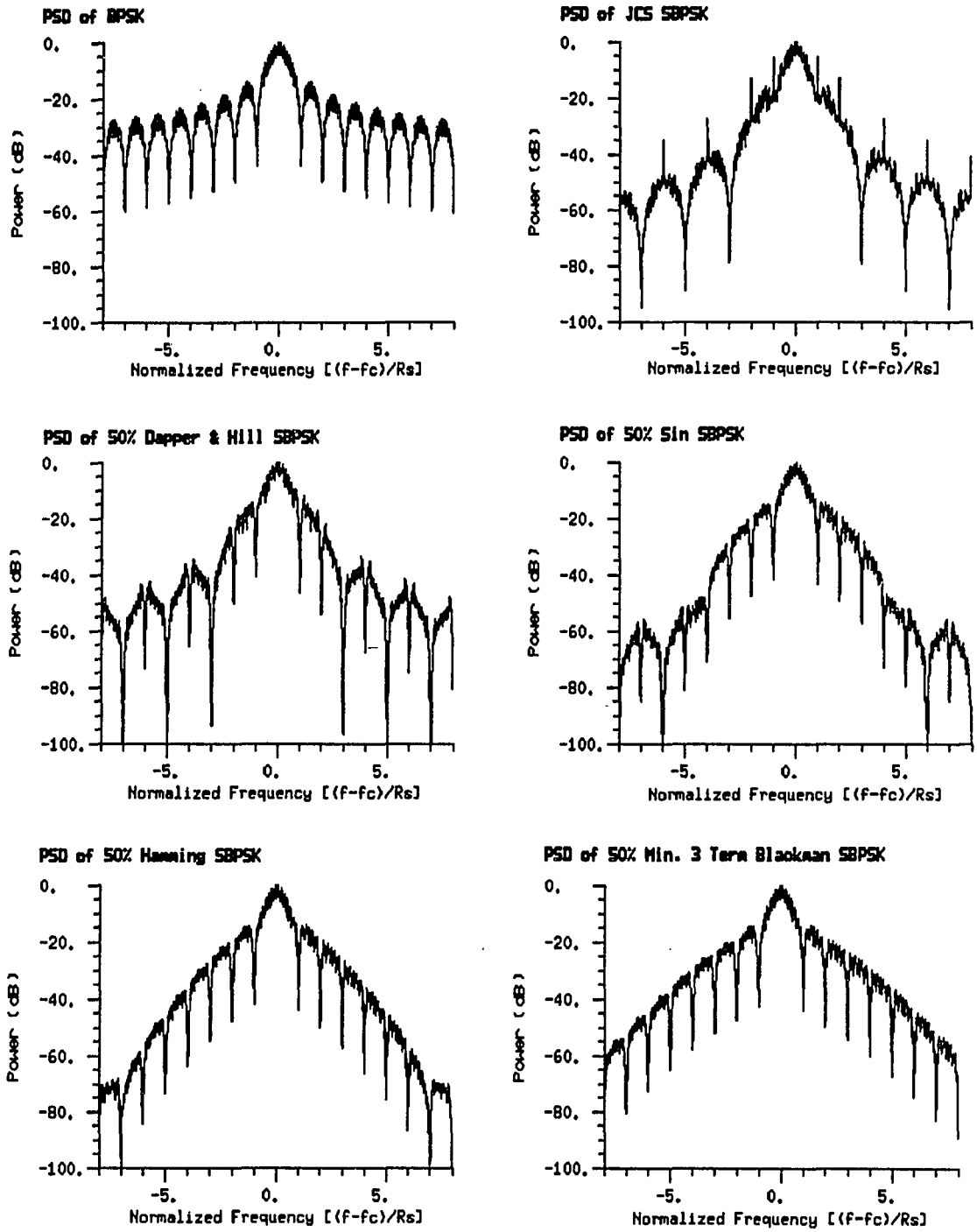

Figure 3.2: Power Spectral Densities of SBPSK Modulations.

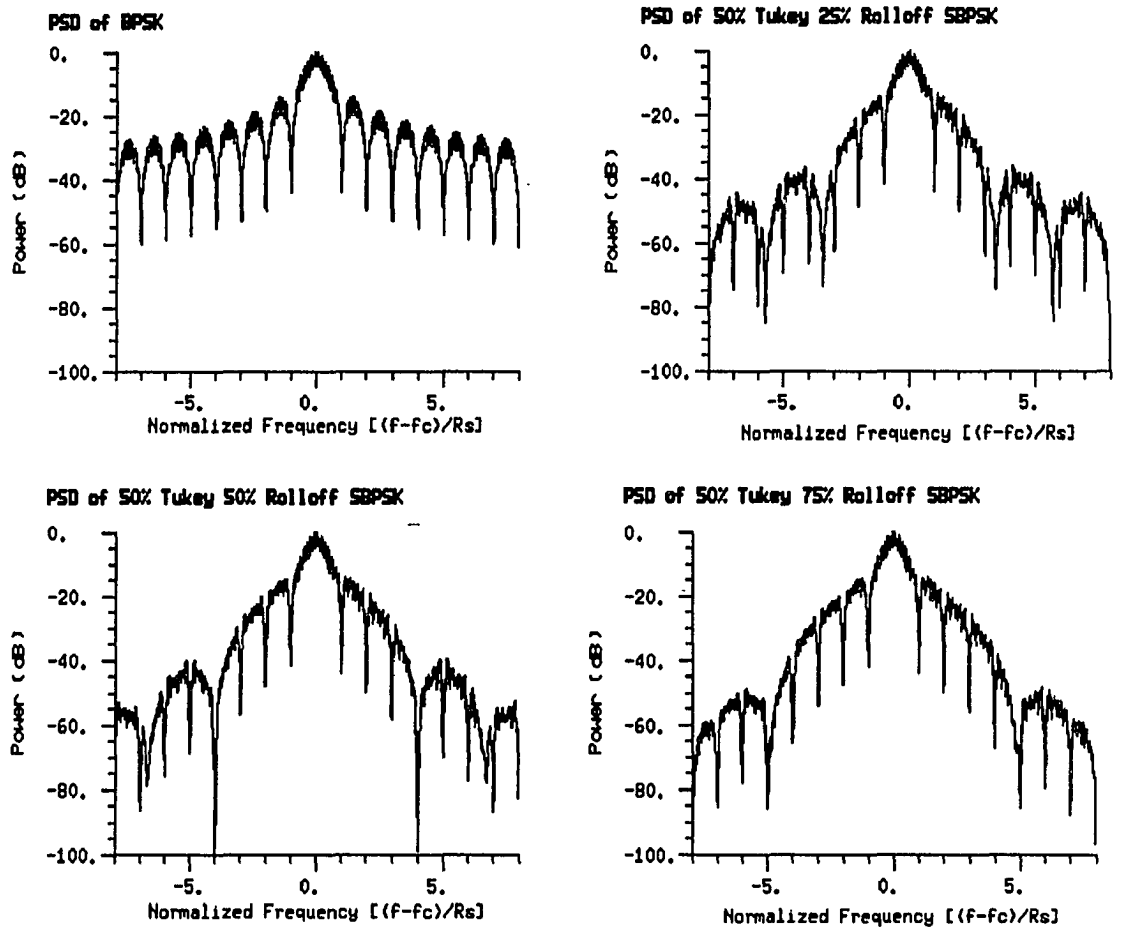

Figure 3.3: Power Spectral Densities of SBPSK Modulations (cont.).

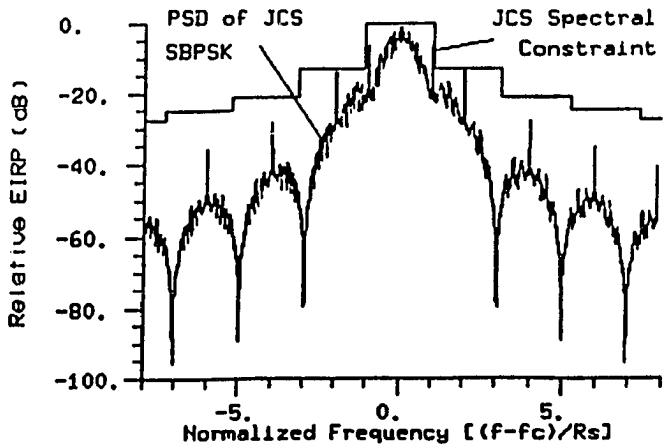

Figure 3.4: PSD of 2400 bps JCS SBPSK and the JCS Spectral Constraint

signal is either 0 or π radians. The mapping $U_{\text{D\&H SBPSK}}$ ensures that Dapper and Hill SBPSK and generalized D&H SBPSK also satisfy this criteria. Recall that the phase of these signals rotates through both halves of the complex plane. To the contrary, the phase of JCS SBPSK is limited to one-half of the complex plane. The result is discrete frequency components called *spectral lines* at integer multiples of the symbol rate.

Figure 3.4 shows that JCS SBPSK transmitted at 2400 bps with a carrier EIRP of 18 dBW does not violate the JCS spectral constraint. This constraint mandates that for signals with carrier EIRP's less than or equal to 18 dBW, the EIRP (relative to the carrier EIRP) of frequencies removed from the carrier not exceed the values shown in the figure. This figure also shows that neither an increase in bit rate nor transmitted power are permissible due to the presence of spectral lines. Also, if the carrier frequency exhibits either a fixed frequency offset relative to the center frequency of the channel or wanders, the JCS constraint is easily violated. Even in the absence of the JCS spectral constraint, modulations such as JCS SBPSK are not recommended for use in situations with nearby adjacent channels. Spectral lines may cause "false-lock" of carrier acquisition circuitry in receivers attempting to demodulate neighboring signals.

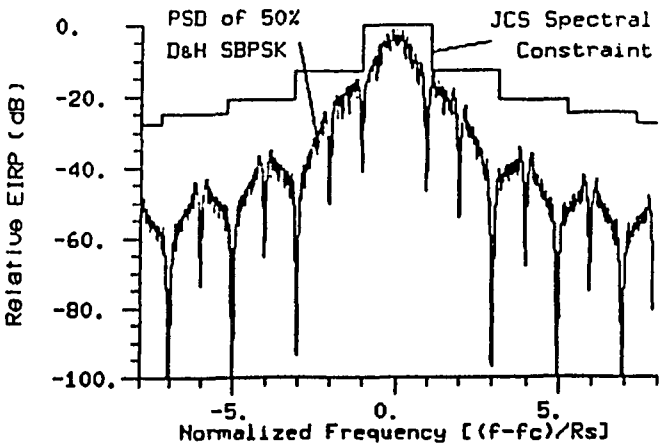

Figure 3.5: PSD of 2400 bps 50% D&H SBPSK and the JCS Spectral Constraint

Figure 3.5 shows that 50% Dapper and Hill SBPSK transmitted at 2400 bps with a carrier EIRP of 18 dBW easily conforms to the spectral criteria established by the JCS. In fact, Figure 3.6 reveals that an increase in the bit rate to 3600 bps is permissible if the carrier EIRP remains at 18 dBW. Alternatively, comparison of Figure 3.7 with Figure 3.5 reveals that 50% D&H SBPSK may be transmitted at an EIRP of 22 dBW when the data rate remains at 2400 bps. This 4 dBW increase in carrier EIRP is obtained from the figures by noting that in both figures, the value of the JCS spectral constraint is 18 dBW at the carrier frequency. In Figure 3.5, the power at the carrier frequency is 4 dBW below the JCS spectral constraint while it is approximately at the JCS spectral constraint in Figure 3.7. Thus for transmitters capable of transmitting at EIRP levels in excess of 18 dBW, shaped modulations enable use of this capability.

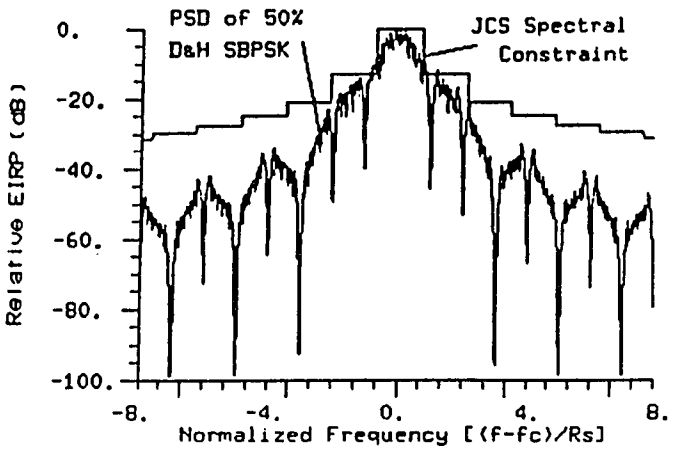

Figure 3.6: PSD of 3600 bps 50% D&H SBPSK and the JCS Spectral Constraint

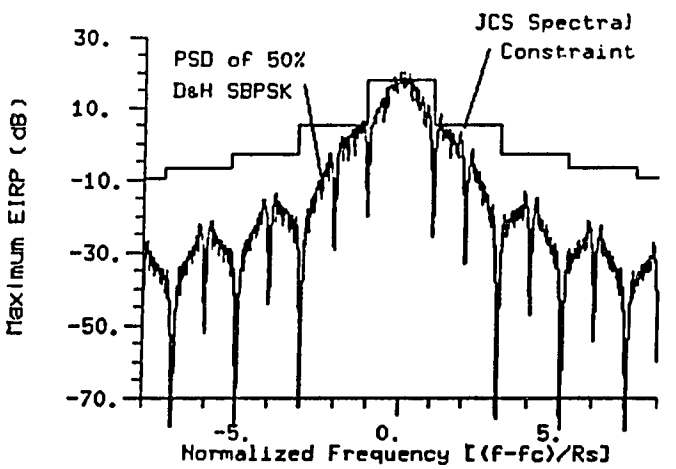

Figure 3.7: PSD of 2400 bps 50% D&H SBPSK with a Carrier EIRP of 22 dBW and the JCS Spectral Constraint

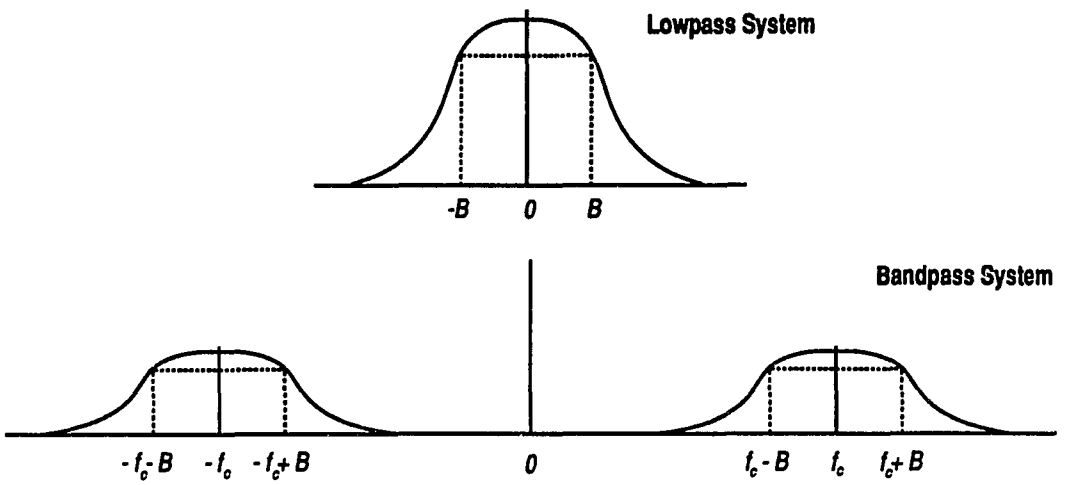

Figure 3.8: The Definition of One-Sided Bandwidth, B.

3.3 Spectral Efficiency of SBPSK Modulations

In the previous section, power spectral densities of SBPSK signals were presented. Examination of these figures reveals that SBPSK modulations appear to be more spectrally efficient than classical BPSK. For SBPSK signals, the power at frequencies far from the carrier frequency are generally lower than the power at the same frequencies for BPSK. The reduction of power at frequencies far from the carrier results from an increase in the amount of power at frequencies near the carrier. Modulations exhibiting this trait are coined "spectrally efficient."

A common method of quantifying spectral efficiency is the fractional out-of-band power curve. These curves present the fraction of the total power outside a given bandwidth. In this section, fractional out-of-band power curves are provided for the modulations being investigated. In all of these figures, the dependent axis displays the fraction of the total power outside a frequency band centered about the carrier frequency. The width of the frequency band (in Hertz) is twice the independent axis value times the transmitted symbol rate, R_s. Hence, the independent axis is in units of normalized one-sided bandwidth. Figure 3.8 illustrates the definition of one-sided bandwidth used throughout this work.

Figure 3.9 is comprised of fractional out-of-band power curves for many of the modulations described in Chapter 2. It is seen that all of the SBPSK modulations are more spectrally efficient than BPSK. In addition, for the small values of bandwidth plotted in these figures, 50% Dapper and Hill SBPSK and JCS SBPSK have the lowest fractional out-of-band power. This results since smoother pulses yield wider mainlobes, and thus, higher out-of-band power for narrow channels. For wider channels (one-sided bandwidth > 2.5 bit rates), fractional out-of-band power is negligible since it is already only 0.3% of the total power for 50% D&H SBPSK at 2.5 bit rates.

Figures 3.10 and 3.11 show the fractional out-of-band power characteristics of BPSK and various SBPSK modulations at the output of a bandpass hardlimiter, an approximation to a typical satellite transponder. The bandpass hardlimiter was implemented by cascading a fifth order Butterworth filter and a hardlimiter. The one-sided filter bandwidth is fixed at R_s Hz in Figure 3.10, and at $0.5R_s$ Hz in Figure 3.11. It is seen that all SBPSK signals show an improvement in spectral containment, while BPSK demonstrates very nearly the same characteristics as it does prior to bandpass hardlimiting.

For SBPSK signals, bandpass hardlimiting results in altered signal phase rotations. As the filter bandwidth narrows, the I and Q channel signals become distorted. This appears as both amplitude modulation and as distortion of the signal phase trajectory. The following limiter removes the AM acquired during filtering, and in doing so, further distorts the signal phase. This process is referred to as *interphasor crosstalk* [32]. Because interphasor crosstalk occurs, the hardlimiter regenerates few of the filtered components of SBPSK signals. As a result, SBPSK signals exhibit lower fractional out-of-band power after bandpass hardlimiting.

When BPSK is filtered, spectral containment is realized by shrinking the phase vector in magnitude which results in AM. The hardlimiter removes the AM, regenerating the filtered components. Although the spectral characteristics of BPSK remain nearly unchanged after bandpass hardlimiting, it should be noted that the signal itself has been degraded. Intersymbol interference introduced

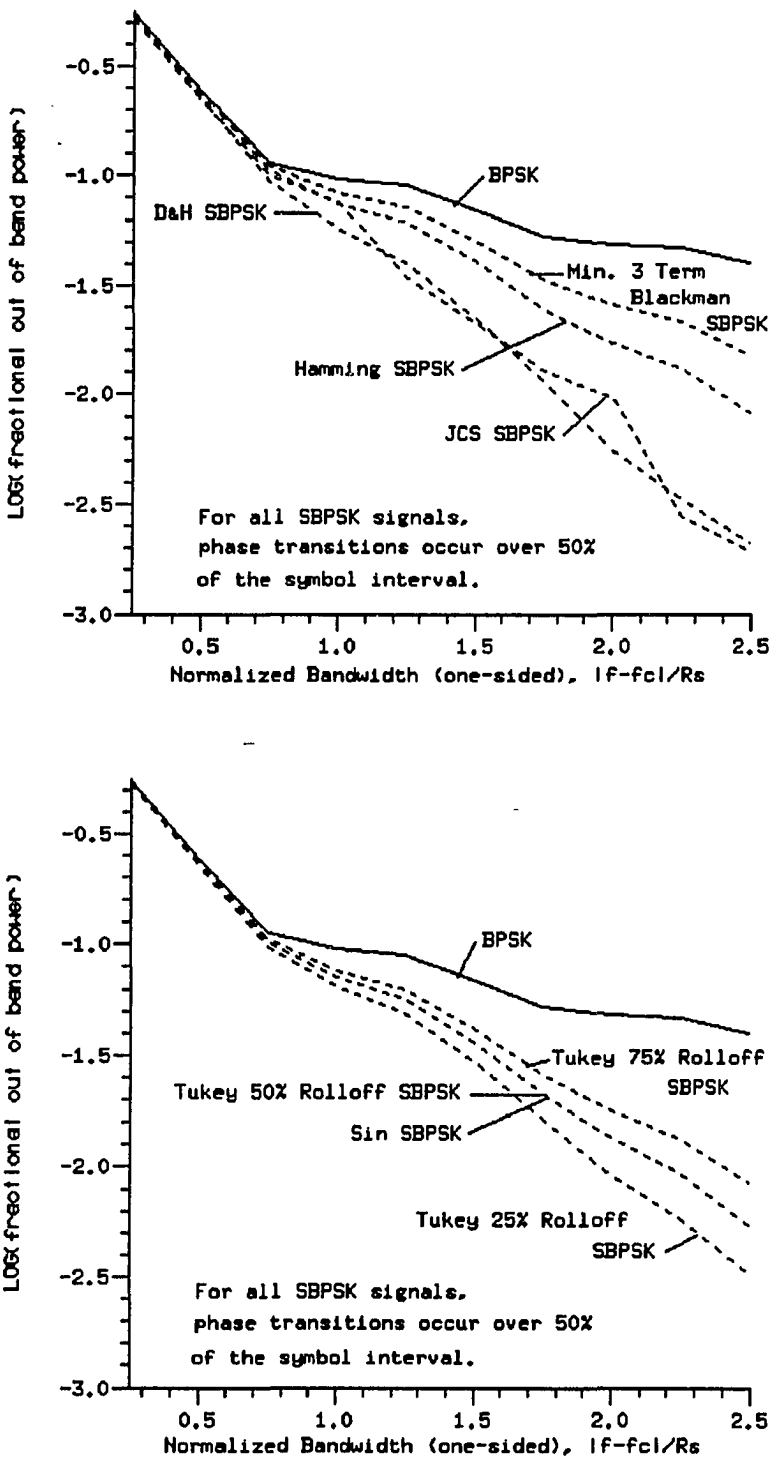

Figure 3.9: Fractional Out-of-Band Power for Various SBPSK Modulations.

by the filtering operation is not removed by the hardlimiter. As a result, it will be seen in Chapter 4 that both BPSK and SBPSK signals experience increased error probability due to bandpass hardlimiting.

In concluding this chapter, several important observations should be summarized. First, 50% Dapper and Hill SBPSK provides a great deal of flexibility in the selection of transmitter bit rate and power without violating the JCS spectral constraint. Second, all the SBPSK signals investigated here exhibit greater spectral containment than BPSK. In particular, D&H SBPSK and JCS SBPSK have the lowest fractional out-of-band power for narrow channels since the mainlobe of a square pulse is the narrowest of the pulse shapes investigated. In addition, SBPSK modulations may be postmodulation filtered to further narrow their power spectrums since subsequent hardlimiting will regenerate few filtered components. This property is generally desirable in systems that hardlimit following postmodulation filtering.

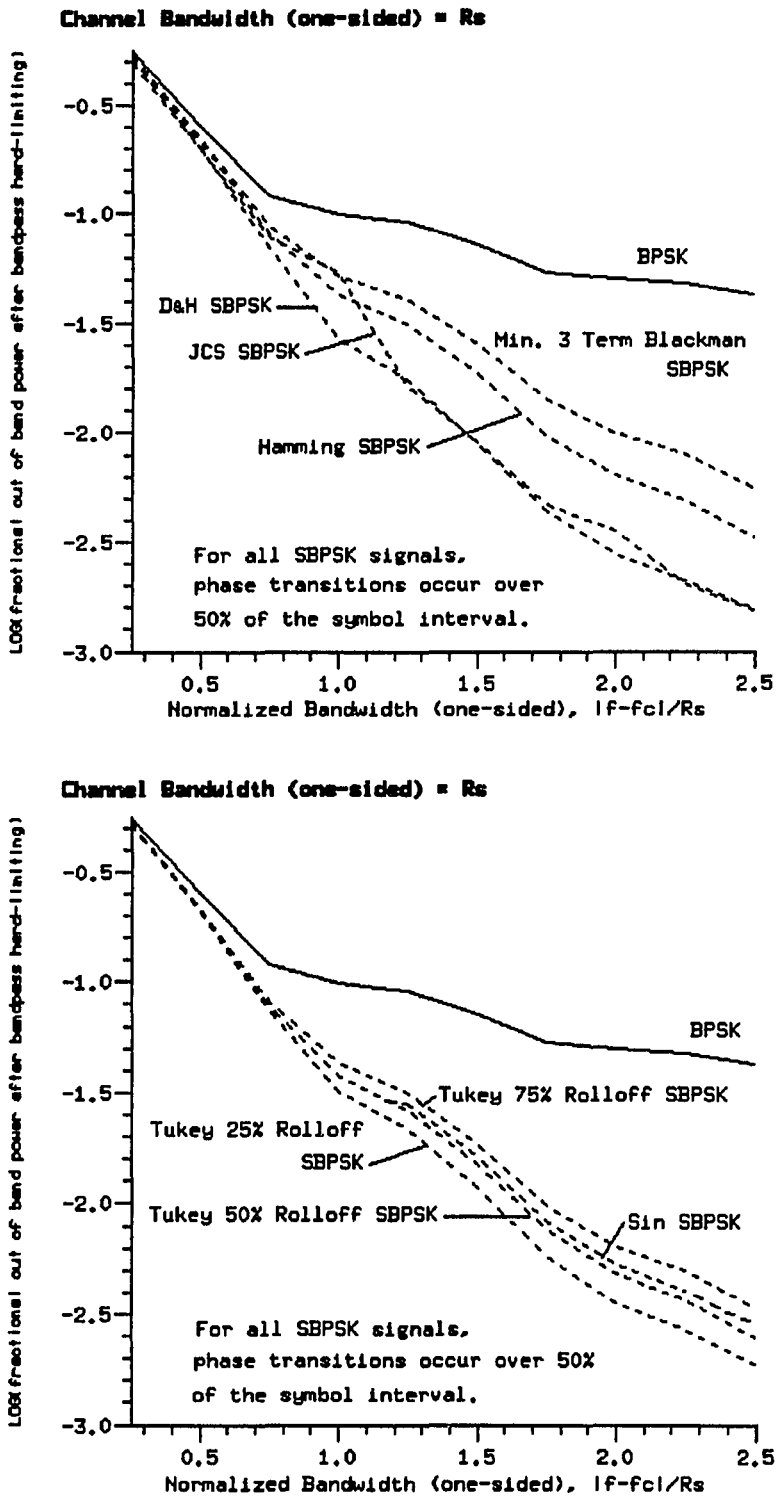

Figure 3.10: Fractional Out-of-Band Power for Bandpass Hardlimited SBPSK.

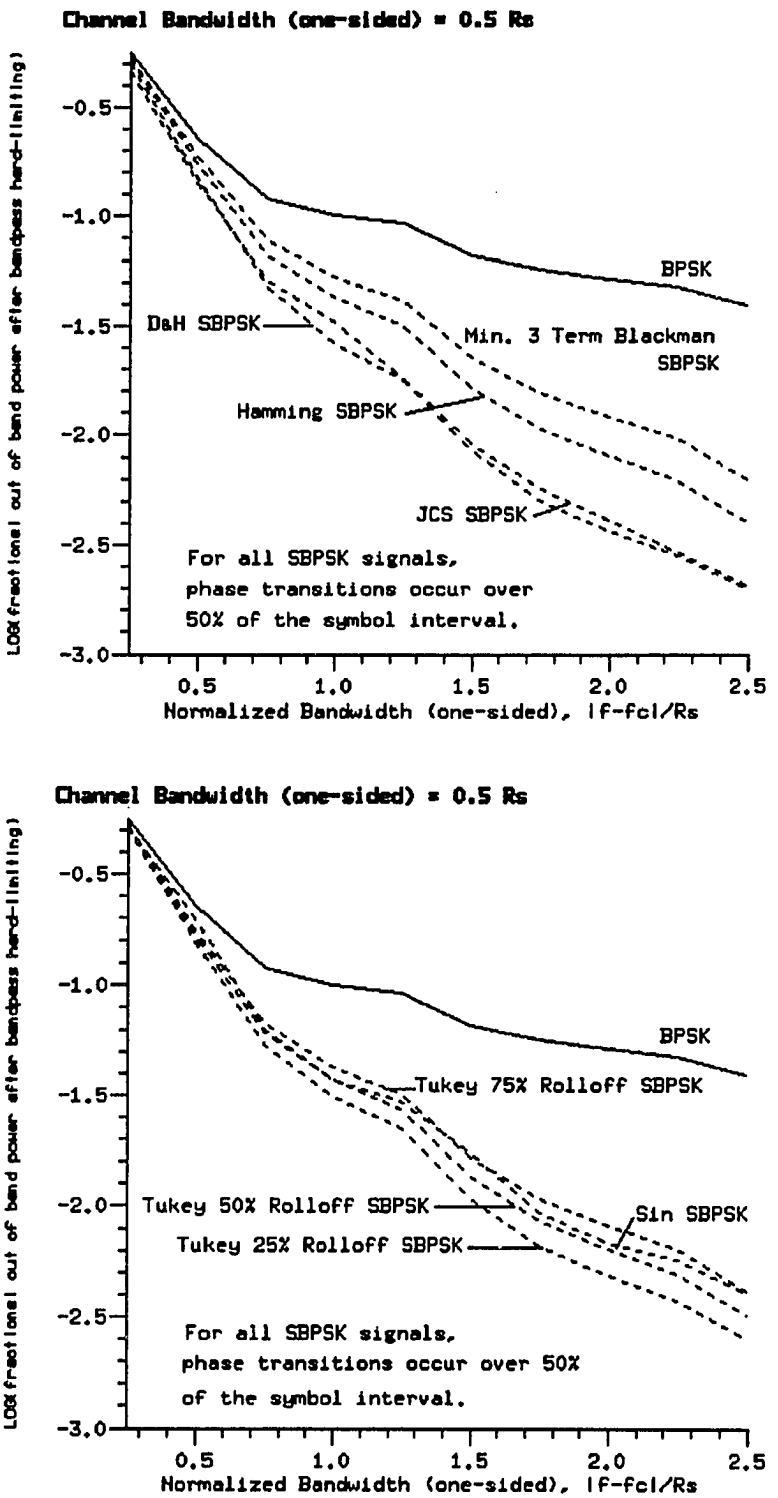

Figure 3.11: Fractional Out-of-Band Power for Bandpass Hardlimited SBPSK (cont.).

CHAPTER 4

Performance of SBPSK Modulations

In previous chapters, SBPSK modulations were introduced and their spectral properties were analyzed. Figures 2.2–2.8 of Chapter 2 demonstrated that signal shaping is accomplished by placing I channel energy into the Q channel. In addition, Figures 3.2 and 3.3 of Chapter 3 showed that the result of shaping is more spectrally efficient modulations. It is seen that the cost of spectral efficiency is the loss of I channel energy. What has yet to be analyzed is how these modulations perform. It is the performance of a modulation that ultimately determines its selection for use in a communication system. The typical measure of performance for a communication system is the probability of error, Pe. In the first section of this chapter, the probability of error will be derived for BPSK signaling and for SBPSK signals demodulated by a BPSK receiver. Curves plotting probability of error vs. signal-to-noise ratio will be presented for BPSK and SBPSK signals. The second section will contain probability of error curves for BPSK and SBPSK signals passed through a bandpass hardlimiter, an approximation to a typical satellite channel. In the final section, the effects of adjacent channel interference on performance will be analyzed.

4.1 Probability of Error

In this section, the probability of error is derived for signals in the presence of zero-mean, stationary, additive white Gaussian noise (AWGN). It is assumed that the channel through which the information is transmitted has no bandwidth limitations. The channel simply attenuates signals

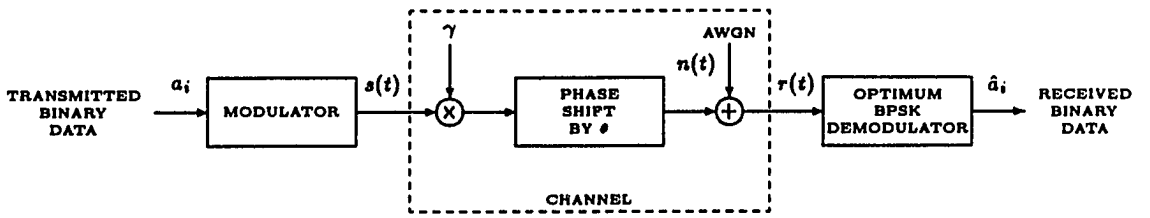

Figure 4.1: A Simple Channel Model.

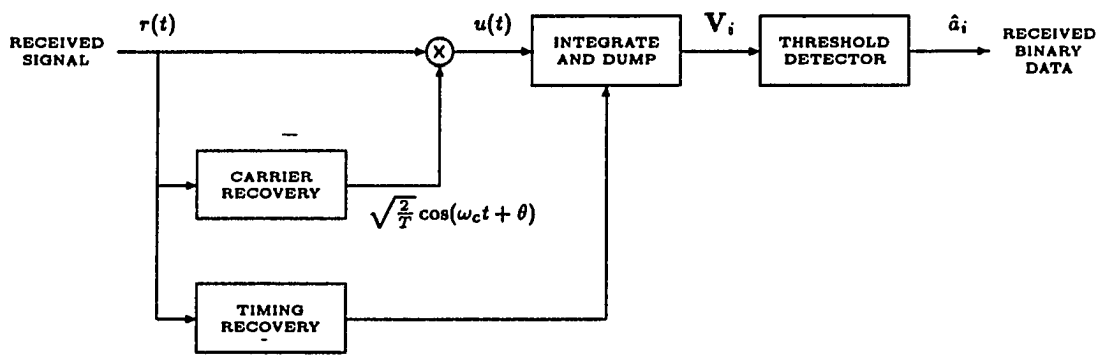

Figure 4.2: A Block Diagram of the Optimum BPSK Demodulator.

passed through it, shifts their phase, and corrupts them by the addition of AWGN. Optimum demodulation for BPSK signaling is also assumed. Optimum BPSK demodulation is accomplished with perfect carrier frequency and phase recovery, as well as perfect symbol timing recovery. Figures 4.1 and 4.2 demonstrate the system being analyzed and the demodulator structure, respectively.

From Chapter 2, the transmitted signal $s(t) = \sqrt{2E/T}\cos[\omega_c t + \phi(t,\alpha)]$. With the channel described above, the received signal has the following form:

$$r(t) = \gamma\sqrt{2E/T}\cos[\omega_c t + \phi(t,\alpha) + \theta] + n(t).$$

where

$$\mathrm{E}[n(t)] = 0 \qquad \text{and} \qquad \mathrm{R}_n(\tau) = \frac{N_0}{2}\delta(\tau).$$

The signal $u(t)$ in Figure 4.2 results from mixing the received waveform with the recovered carrier. Thus,

$$\begin{aligned} u(t) &= r(t) \cdot \sqrt{\frac{2}{T}} \cos(\omega_c t + \theta) \\ &= \frac{\gamma\sqrt{E}}{T} \{\cos[\phi(t,\alpha)] + \cos[2(\omega_c t + \theta) + \phi(t,\alpha)]\} + \sqrt{\frac{2}{T}} n(t) \cos(\omega_c t + \theta). \end{aligned}$$

When ideal timing recovery is achieved, the phase difference between the recovered clock at the demodulator and the baseband I channel signal (referred to as the I channel signal) is zero. Figure 4.3 demonstrates ideal timing recovery for BPSK signaling. Notice that not only is the frequency of the recovered clock $\frac{1}{T}$, but that the recovered clock and the I channel signal are exactly in phase. As a result, the integrate and dump circuit will perform the integration of $u(t)$ over exactly one symbol. When the same demodulator is used for SBPSK signals, ideal timing recovery is shown in Figure 4.4. Notice that for SBPSK signals with the pulse shape $g(t)$ symmetric about $\frac{\lambda T}{2}$, the recovered clock is delayed by $\frac{\lambda T}{2}$ seconds with respect to the transmitter clock. The timing recovery circuit shifts the definition of the beginning and end of symbols to maintain a zero phase difference between the recovered clock and the I channel signal. In this case, the integrate and dump circuit will perform the integration of $u(t)$ over portions of two symbols. In Figures 4.3 and 4.4, as well as the discussion that follows, the use of "′" indicates symbol timing as defined by the recovered clock at the demodulator. The absence of "′" indicates timing as defined by the transmitter.

For both BPSK and SBPSK, the integrate and dump output appears as a stochastic process, v(t). During the $i+1^{\text{th}}$ data interval, the integrate and dump output is the random variable $\mathbf{V}_i$. In other words,

$$v(t) = \mathbf{V}_i \quad \text{for } (i+1)T' \leq t < (i+2)T'$$

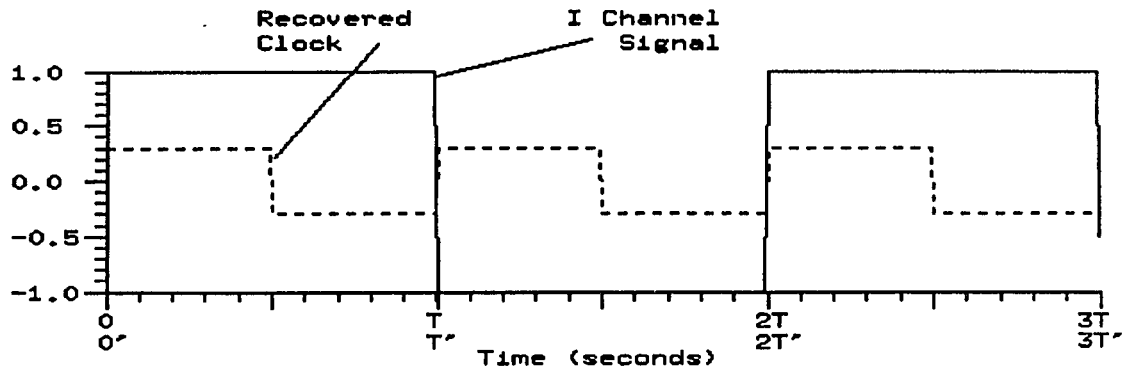

Figure 4.3: Ideal Timing Recovery for BPSK Signaling.

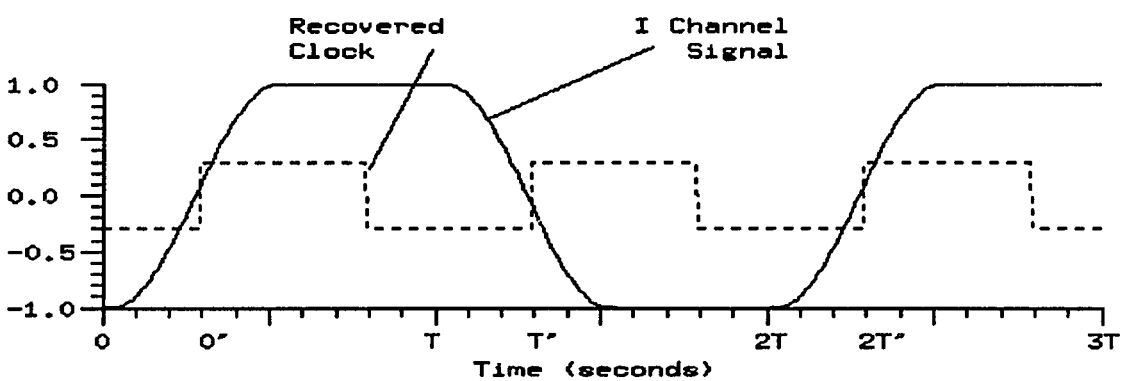

Figure 4.4: Ideal Timing Recovery for SBPSK Signaling.

where

$$\begin{aligned}
\mathbf{V}_i &= \int_{iT'}^{(i+1)T'} u(t)\,dt \\
&= \underbrace{\frac{\gamma\sqrt{E}}{T}\int_{iT'}^{(i+1)T'} \cos[\phi(t,\alpha)]\,dt}_{\mathbf{X}_i} + \underbrace{\frac{\gamma\sqrt{E}}{T}\int_{iT'}^{(i+1)T'} \cos[2(\omega_c t+\theta)+\phi(t,\alpha)]\,dt}_{\mathbf{Y}_i} \\
&+ \underbrace{\sqrt{\frac{2}{T}}\int_{iT'}^{(i+1)T'} n(t)\cos(\omega_c t+\theta)\,dt}_{\mathbf{Z}_i}. \qquad (4.1)
\end{aligned}$$

Let us analyze each term of this equation.

$\mathbf{X}_i$ is the integration of the I channel signal over the i^{th} received symbol interval. It is a random variable whose value is dependent upon the transmitted data sequence. For BPSK signaling, the transmitter and receiver clocks are in phase ($t' = t$.) As a result, $\mathbf{X}_i$ takes one of two possible values based upon the i^{th} transmitted data bit. From Chapter 2, $\phi(t,\alpha)$ is 0 radians when $a_i = -1$ and π radians when $a_i = +1$. Consequently,

$$\mathbf{X}_i = \frac{\gamma\sqrt{E}}{T}\int_{iT}^{(i+1)T} \cos[\phi(t,\alpha)]\,dt = \begin{cases} \gamma\sqrt{E} & \text{if } a_i = -1 \\ -\gamma\sqrt{E} & \text{if } a_i = +1. \end{cases}$$

For SBPSK signaling, the receiver clock is delayed $\frac{\lambda T}{2}$ seconds with respect to the transmitter clock ($t' = t + \frac{\lambda T}{2}$.) Hence,

$$\begin{aligned}
\mathbf{X}_i &= \frac{\gamma\sqrt{E}}{T}\int_{iT+\frac{\lambda T}{2}}^{(i+1)T+\frac{\lambda T}{2}} \cos[\phi(t,\alpha)]\,dt \\
&= \gamma\sqrt{E}\left[\underbrace{\frac{1}{T}\int_{iT+\frac{\lambda T}{2}}^{iT+\lambda T} \cos[\phi(t,\alpha)]\,dt}_{\mathbf{A}_i} + \underbrace{\frac{1}{T}\int_{iT+\lambda T}^{(i+1)T} \cos[\phi(t,\alpha)]\,dt}_{\mathbf{B}_i}\right. \\
&\qquad \left. + \underbrace{\frac{1}{T}\int_{(i+1)T}^{(i+1)T+\frac{\lambda T}{2}} \cos[\phi(t,\alpha)]\,dt}_{\mathbf{C}_i}\right]. \qquad (4.2)
\end{aligned}$$

When $g(t)$ is symmetric about $\frac{\lambda T}{2}$, $\mathbf{X}_i$ takes one of six possible values based upon the sequence $\{a_{i-1}, a_i, a_{i+1}\}$. These values are listed below:

$$\mathbf{X}_i = \begin{cases} \gamma\sqrt{E} & \text{for } \{-1,-1,-1\} \\ \gamma\sqrt{E}(1-\frac{\lambda}{2}) + \frac{\gamma\sqrt{E}}{T}\int_0^{\frac{\lambda T}{2}} \cos(2\pi\int_0^t g(\tau)\,d\tau)\,dt & \text{for } \{-1,-1,+1\} \text{ or } \{+1,-1,-1\} \\ \gamma\sqrt{E}(1-\lambda) + 2\frac{\gamma\sqrt{E}}{T}\int_0^{\frac{\lambda T}{2}} \cos(2\pi\int_0^t g(\tau)\,d\tau)\,dt & \text{for } \{+1,-1,+1\} \\ -\left[\gamma\sqrt{E}(1-\lambda) + 2\frac{\gamma\sqrt{E}}{T}\int_0^{\frac{\lambda T}{2}} \cos(2\pi\int_0^t g(\tau)\,d\tau)\,dt\right] & \text{for } \{-1,+1,-1\} \\ -\left[\gamma\sqrt{E}(1-\frac{\lambda}{2}) + \frac{\gamma\sqrt{E}}{T}\int_0^{\frac{\lambda T}{2}} \cos(2\pi\int_0^t g(\tau)\,d\tau)\,dt\right] & \text{for } \{+1,+1,-1\} \text{ or } \{-1,+1,+1\} \\ -\gamma\sqrt{E} & \text{for } \{+1,+1,+1\}. \end{cases} \tag{4.3}$$

Figure 4.5 shows how these values are obtained. The terms $\mathbf{A}_i$, $\mathbf{B}_i$, and $\mathbf{C}_i$ of equation (4.2) correspond to the area of regions a, b, and c, respectively. Regions a and c are "transition" regions. The signal phase will rotate during region a if $a_{i-1} \neq a_i$ and during region c if $a_i \neq a_{i+1}$. When phase rotations occur, the I channel signal exhibits transitions in polarity. $\mathbf{A}_i$ takes one of four possible values. If $a_{i-1} = a_i = -1$, the signal phase remains stationary at 0 radians and

$$\mathbf{A}_i = \frac{1}{T}\int_{iT+\frac{\lambda T}{2}}^{iT+\lambda T} \cos(0)\,dt = \frac{\lambda}{2}.$$

Similarly, when $a_{i-1} = a_i = +1$, $\mathbf{A}_i = \frac{-\lambda}{2}$. When $a_{i-1} = +1$ and $a_i = -1$, the signal phase rotates from π radians to 0 radians, and

$$\begin{aligned} \mathbf{A}_i &= \frac{1}{T}\int_{iT+\frac{\lambda T}{2}}^{iT+\lambda T} \cos[\phi(t,\alpha)]\,dt \\ &= \frac{1}{T}\int_{iT+\frac{\lambda T}{2}}^{iT+\lambda T} \cos\left[2\pi h\sum_{k=-\infty}^{\infty}\alpha_k q(t-kT)\right]dt \\ &= \frac{1}{T}\int_{iT+\frac{\lambda T}{2}}^{iT+\lambda T} \cos\left[2\pi\sum_{k=-\infty}^{i-1}\alpha_k q(t-kT)\right. \\ &+ \left. 2\pi\alpha_i q(t-iT) + 2\pi\sum_{k=i+1}^{\infty}\alpha_k q(t-kT)\right]dt \qquad (4.4) \\ &= \frac{1}{T}\int_{iT+\frac{\lambda T}{2}}^{iT+\lambda T} \cos\left[\pi + 2\pi q(t-iT)\right]dt. \qquad (4.5) \end{aligned}$$

$a_{i-1} = -1,\ a_i = -1,\ a_{i+1} = -1$

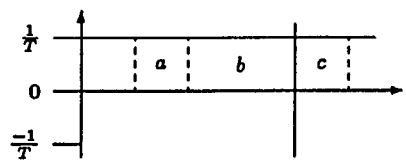

$\mathbf{A}_i = \frac{\lambda}{2}$

$\mathbf{B}_i = (1 - \lambda)$

$\mathbf{C}_i = \frac{\lambda}{2}$

$a_{i-1} = -1,\ a_i = -1,\ a_{i+1} = +1$

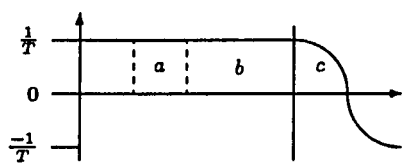

$\mathbf{A}_i = \frac{\lambda}{2}$

$\mathbf{B}_i = (1 - \lambda)$

$\mathbf{C}_i = \frac{1}{T}\int_0^{\frac{\lambda T}{2}} \cos\left(2\pi \int_0^t g(\tau)\, d\tau\right) dt$

$a_{i-1} = +1,\ a_i = -1,\ a_{i+1} = -1$

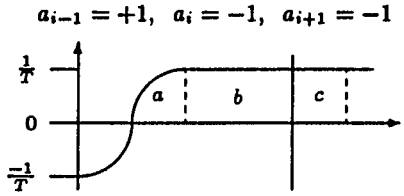

$\mathbf{A}_i = \frac{1}{T}\int_0^{\frac{\lambda T}{2}} \cos\left(2\pi \int_0^t g(\tau)\, d\tau\right) dt$

$\mathbf{B}_i = (1 - \lambda)$

$\mathbf{C}_i = \frac{\lambda}{2}$

$a_{i-1} = +1,\ a_i = -1,\ a_{i+1} = +1$

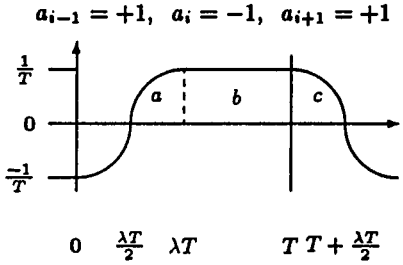

$\mathbf{A}_i = \frac{1}{T}\int_0^{\frac{\lambda T}{2}} \cos\left(2\pi \int_0^t g(\tau)\, d\tau\right) dt$

$\mathbf{B}_i = (1 - \lambda)$

$\mathbf{C}_i = \frac{1}{T}\int_0^{\frac{\lambda T}{2}} \cos\left(2\pi \int_0^t g(\tau)\, d\tau\right) dt$

All polarities may be reversed to obtain the remaining four combinations.

Figure 4.5: Piecewise Calculation of $\mathbf{X}_i$ for SBPSK Signals.

Equation (4.5) is obtained from (4.4) because the cumulative phase at the end of the $i-1^{\text{th}}$ symbol must equal π radians since $a_{i-1} = +1$. Also, since $q(t)$ is causal, the contribution to the phase due to future bits is zero. Finally the polarity of α_i is inconsequential since $\cos(\pi + \theta) = \cos(\pi - \theta)$. Substituting the definition of $q(t)$ into (4.5) yields

$$\mathbf{A}_i = \frac{1}{T}\int_{iT+\frac{\lambda T}{2}}^{iT+\lambda T} \cos\left[\pi + 2\pi\int_0^{t-iT} g(\tau)\,d\tau\right] dt.$$

By a change of variables with $v = t - iT - \frac{\lambda T}{2}$,

$$\mathbf{A}_i = \frac{1}{T}\int_0^{\frac{\lambda T}{2}} \cos\left[\pi + 2\pi\int_0^{v+\frac{\lambda T}{2}} g(\tau)\,d\tau\right] dv.$$

Since $g(\tau)$ is symmetric about $\frac{\lambda T}{2}$ and integrates to $\frac{1}{2}$,

$$\mathbf{A}_i = \frac{1}{T}\int_0^{\frac{\lambda T}{2}} \cos\left[\pi + 2\pi\left\{\frac{1}{2} - \int_0^{\frac{\lambda T}{2}-v} g(\tau)\,d\tau\right\}\right] dv.$$

A second change of variables with $t = \frac{\lambda T}{2} - v$ gives

$$\mathbf{A}_i = -\frac{1}{T}\int_{\frac{\lambda T}{2}}^{0} \cos\left[\pi + 2\pi\left\{\frac{1}{2} - \int_0^{t} g(\tau)\,d\tau\right\}\right] dt.$$

And finally,

$$\mathbf{A}_i = \frac{1}{T}\int_0^{\frac{\lambda T}{2}} \cos\left[2\pi\int_0^{t} g(\tau)\,d\tau\right] dt \quad \text{if } a_{i-1} = +1 \text{ and } a_i = -1.$$

Similarly,

$$\mathbf{A}_i = -\frac{1}{T}\int_0^{\frac{\lambda T}{2}} \cos\left[2\pi\int_0^{t} g(\tau)\,d\tau\right] dt \quad \text{if } a_{i-1} = -1 \text{ and } a_i = +1.$$

It can be shown that $\mathbf{C}_i$ takes the same four values. Finally, $\mathbf{B}_i$ takes one of two values based upon the current data bit. When $a_i = -1$, the signal phase reaches π radians by time $t = iT + \lambda T$ and stays at this value throughout the remainder of the bit interval. For $a_i = +1$, the signal phase remains stationary at 0 radians. Consequently,

$$\mathbf{B}_i = \begin{cases} \frac{1}{T}\int_{iT+\lambda T}^{(i+1)T} \cos(\pi)\,dt = 1-\lambda & \text{if } a_i = -1 \\ \frac{1}{T}\int_{iT+\lambda T}^{(i+1)T} \cos(0)\,dt = -(1-\lambda) & \text{if } a_i = +1. \end{cases}$$

Figure 4.5 demonstrates four of the eight possible combinations of $\mathbf{A}_i$, $\mathbf{B}_i$, and $\mathbf{C}_i$. By adding these values, the six possible values of $\mathbf{X}_i$ given in equation (4.3) are obtained. We can then conclude that for both BPSK and SBPSK, $\mathbf{X}_i$ is deterministic when *conditioned* on specific data. That is, $\mathrm{E}[\mathbf{X}_i|a_i]$ is known for BPSK and $\mathrm{E}[\mathbf{X}_i|a_{i-1}, a_i, a_{i+1}]$ is known for SBPSK.

The second term of equation (4.1), $\mathbf{Y}_i$, is a random variable representing the integration of the double frequency component of a waveform after mixing. Since the carrier frequency of a modulated signal is generally much larger than the transmitted symbol rate, it is assumed that $\omega_c \gg 1/T \gg 1$. When this is true, $\mathbf{Y}_i$ is negligible. This is shown below.

$$\begin{aligned}
\mathbf{Y}_i &= \frac{\gamma\sqrt{E}}{T}\int_{iT'}^{(i+1)T'} \cos[2(\omega_c t+\theta)+\phi(t,\alpha)]\,dt \\
&= \frac{\gamma\sqrt{E}}{T}\int_{iT'}^{(i+1)T'} \cos[\phi(t,\alpha)]\cos[2(\omega_c t+\theta)]\,dt \\
&- \frac{\gamma\sqrt{E}}{T}\int_{iT'}^{(i+1)T'} \sin[\phi(t,\alpha)]\sin[2(\omega_c t+\theta)]\,dt.
\end{aligned}$$

Since $\omega_c \gg 1/T$, $\cos[\phi(t,\alpha)]$ and $\sin[\phi(t,\alpha)]$ may be considered the constants C_1 and C_2, respectively. This yields

$$\begin{aligned}
\mathbf{Y}_i &= \frac{\gamma\sqrt{E}}{T}C_1\,\frac{\sin[2(\omega_c t+\theta)]}{2\omega_c}\Bigg|_{iT'}^{(i+1)T'} + \frac{\gamma\sqrt{E}}{T}C_2\,\frac{\cos[2(\omega_c t+\theta)]}{2\omega_c}\Bigg|_{iT'}^{(i+1)T'} \\
&\approx 0.
\end{aligned}$$

$\mathbf{Z}_i$ represents the output of the integrate and dump circuit due to the presence of AWGN modulated by the recovered carrier. $\mathbf{Z}_i$ is a zero-mean, Gaussian RV since the stochastic process $n(t)$ is zero-mean and Gaussian. The mean and variance of $\mathbf{Z}_i$ are calculated below.

$$\begin{aligned}
m_{Z_i} &= \mathrm{E}\left[\sqrt{\frac{2}{T}}\int_{iT'}^{(i+1)T'} n(t)\cos(\omega_c t+\theta)\,dt\right] \\
&= \sqrt{\frac{2}{T}}\int_{iT'}^{(i+1)T'} \mathrm{E}[n(t)]\cos(\omega_c t+\theta)\,dt \;=\; 0.
\end{aligned}$$

Also,

$$\sigma_{Z_i} = \mathrm{E}[(\mathbf{Z}_i - m_{Z_i})^2] = \mathrm{E}[\mathbf{Z}_i^2]$$

$$
\begin{aligned}
&= \frac{2}{T}\int_{iT'}^{(i+1)T'}\int_{iT'}^{(i+1)T'} \mathrm{E}[n(t)n(\tau)]\cos(\omega_c t+\theta)\cos(\omega_c \tau+\theta)\,dt\,d\tau \\
&= \frac{2}{T}\int_{iT'}^{(i+1)T'}\int_{iT'}^{(i+1)T'} R_n(t-\tau)\cos(\omega_c t+\theta)\cos(\omega_c \tau+\theta)\,dt\,d\tau \\
&= \frac{2}{T}\int_{iT'}^{(i+1)T'}\int_{iT'}^{(i+1)T'} \frac{N_0}{2}\delta(t-\tau)\cos(\omega_c t+\theta)\cos(\omega_c \tau+\theta)\,dt\,d\tau \\
&= \frac{N_0}{T}\int_{iT'}^{(i+1)T'} \cos^2(\omega_c t+\theta)\,dt \\
&= \frac{N_0}{T}\int_{iT'}^{(i+1)T'} \frac{1}{2}[1+\cos[2(\omega_c t+\theta)]]\,dt \\
&= \frac{N_0}{2}.
\end{aligned}
$$

Note that the contribution of the double frequency term was ignored since ω_c is very large.

At this point, it is helpful to summarize what has recently been found. The integrate and dump output during the $i+1^{\text{th}}$ bit interval is the random variable $\mathbf{V}_i$. $\mathbf{V}_i$ is comprised of three terms with the second term, $\mathbf{Y}_i$, approximately zero. $\mathbf{X}_i$ is a discrete RV taking known values when conditioned on the transmitted data a_{i-1}, a_i and a_{i+1}. $\mathbf{Z}_i$ is a zero-mean, Gaussian RV with variance $\frac{N_0}{2}$. Thus, $\mathbf{V}_i$ is a Gaussian random variable with variance $\frac{N_0}{2}$ and known mean when conditioned on a_{i-1}, a_i and a_{i+1}. Its probability density function is given by

$$
f_{\mathbf{V}_i|a_{i-1},a_i,a_{i+1}}(v) = \frac{1}{\sqrt{2\pi\frac{N_0}{2}}} e^{-\frac{1}{2}\frac{(v-\mathrm{E}[\mathbf{X}_i|a_{i-1},a_i,a_{i+1}])^2}{N_0/2}}.
$$

The remaining step of the demodulation process is the decision of $\hat{a}_i$ based upon $\mathbf{V}_i$. For BPSK, the mean of $\mathbf{V}_i$ is either $\gamma\sqrt{E}$ or $-\gamma\sqrt{E}$ if $a_i = -1$ or $+1$, respectively. If the data bits are equally likely, it is intuitively satisfying to say that the demodulator should choose $\hat{a}_i = -1$ when $\mathbf{V}_i$ is any value greater than zero, and choose $\hat{a}_i = +1$ if $\mathbf{V}_i$ is less than zero. When $\mathbf{V}_i$ is exactly zero, the choice of $\hat{a}_i$ is arbitrary. In fact, this is the case for the optimum BPSK demodulator.

From the knowledge acquired, it is now possible to calculate the probability of error. Since the modulations of interest are binary, the probability of symbol error and the probability of bit error are synonymous and denoted simply as Pe. Using Bayes' Rule, the probability of error may be

expressed as

$$\begin{aligned} \text{Pe} &= \text{P}\{\hat{a}_i = -1 | a_i = +1\} \cdot \text{P}\{a_i = +1\} + \text{P}\{\hat{a}_i = +1 | a_i = -1\} \cdot \text{P}\{a_i = -1\} \\ &= \frac{1}{2}[\text{P}\{\hat{a}_i = -1 | a_i = +1\} + \text{P}\{\hat{a}_i = +1 | a_i = -1\}] \end{aligned} \tag{4.6}$$

since both $a_i = +1$ and $a_i = -1$ are equally likely. For BPSK,

$$\begin{aligned} \text{P}\{\hat{a}_i = -1 | a_i = +1\} &= \text{P}\{\text{V}_i > 0 | a_i = +1\} \\ &= \int_0^\infty \frac{1}{\sqrt{2\pi N_0/2}} e^{-\frac{1}{2}\frac{(v+\gamma\sqrt{E})^2}{N_0/2}} dv \\ &= \int_0^\infty \frac{1}{\sqrt{2\pi N_0/2}} e^{-\frac{1}{2}(\frac{v+\gamma\sqrt{E}}{\sqrt{N_0/2}})^2} dv \\ &= \int_{\frac{\gamma\sqrt{E}}{\sqrt{N_0/2}}}^\infty \frac{1}{\sqrt{2\pi}} e^{-\frac{1}{2}u^2} du \end{aligned}$$

by a change of variables with $u = \frac{v+\gamma\sqrt{E}}{\sqrt{N_0/2}}$. This integration cannot be performed analytically. It has been solved via numerical methods and is known as the "Q" function. Specifically, $Q(x) = \frac{1}{\sqrt{2\pi}} \int_x^\infty e^{-\frac{1}{2}\zeta^2} d\zeta$. Thus,

$$\text{P}\{\hat{a}_i = -1 | a_i = +1\} = Q\left(\sqrt{\frac{\gamma^2 E}{N_0/2}}\right). \tag{4.7}$$

Similarly,

$$\text{P}\{\hat{a}_i = +1 | a_i = -1\} = \text{P}\{\text{V}_i \leq 0 | a_i = -1\} = Q\left(\sqrt{\frac{\gamma^2 E}{N_0/2}}\right). \tag{4.8}$$

Substituting (4.7) and (4.8) into (4.6) gives the well known probability of error for BPSK

$$\text{Pe}_{\text{BPSK}} = Q\left(\sqrt{\frac{\gamma^2 E}{N_0/2}}\right). \tag{4.9}$$

For SBPSK,

$$\begin{aligned} \text{P}\{\hat{a}_i = -1 | a_i = +1\} &= \text{P}\{\text{V}_i > 0 | a_i = +1\} \\ &= \text{P}\{\text{V}_i > 0 | a_{i-1} = -1, a_i = +1, a_{i+1} = -1\} \cdot \text{P}\{a_{i-1} = -1, a_{i+1} = -1\} \\ &+ \text{P}\{\text{V}_i > 0 | a_{i-1} = -1, a_i = +1, a_{i+1} = +1\} \cdot \text{P}\{a_{i-1} = -1, a_{i+1} = +1\} \\ &+ \text{P}\{\text{V}_i > 0 | a_{i-1} = +1, a_i = +1, a_{i+1} = -1\} \cdot \text{P}\{a_{i-1} = +1, a_{i+1} = -1\} \end{aligned}$$

$$
\begin{aligned}
&+ \quad \mathrm{P}\{\mathrm{V}_i > 0 | a_{i-1} = +1, a_i = +1, a_{i+1} = +1\} \cdot \mathrm{P}\{a_{i-1} = +1, a_{i+1} = +1\} \\
&= \quad \frac{1}{4}\left[\int_0^\infty \frac{1}{\sqrt{2\pi N_0/2}} e^{-\frac{1}{2}\frac{\{v+[\gamma\sqrt{E}(1-\lambda)+2\frac{\gamma\sqrt{E}}{T}\int_0^{\frac{\lambda T}{2}}\cos(2\pi\int_0^t g(\tau)\,d\tau)\,dt]\}^2}{N_0/2}} dv\right. \\
&+ \quad 2\int_0^\infty \frac{1}{\sqrt{2\pi N_0/2}} e^{-\frac{1}{2}\frac{\{v+[\gamma\sqrt{E}(1-\frac{\lambda}{2})+\frac{\gamma\sqrt{E}}{T}\int_0^{\frac{\lambda T}{2}}\cos(2\pi\int_0^t g(\tau)\,d\tau)\,dt]\}^2}{N_0/2}} dv \\
&+ \quad \left.\int_0^\infty \frac{1}{\sqrt{2\pi N_0/2}} e^{-\frac{1}{2}\frac{\{v+\gamma\sqrt{E}\}^2}{N_0/2}} dv\right] \\
&= \quad \frac{1}{4}Q\left(\sqrt{\frac{\gamma^2 E}{N_0/2}\left\{(1-\lambda)+\frac{2}{T}\int_0^{\frac{\lambda T}{2}}\cos\left(2\pi\int_0^t g(\tau)\,d\tau\right)\,dt\right\}^2}\right) \\
&+ \quad \frac{1}{2}Q\left(\sqrt{\frac{\gamma^2 E}{N_0/2}\left\{(1-\frac{\lambda}{2})+\frac{1}{T}\int_0^{\frac{\lambda T}{2}}\cos\left(2\pi\int_0^t g(\tau)\,d\tau\right)\,dt\right\}^2}\right) \\
&+ \quad \frac{1}{4}Q\left(\sqrt{\frac{\gamma^2 E}{N_0/2}}\right). \qquad (4.10)
\end{aligned}
$$

The same result is obtained for $\mathrm{P}\{\hat{a}_i = +1 | a_i = -1\}$. Substituting (4.10) into (4.6) twice yields the probability of error for SBPSK as

$$
\begin{aligned}
\mathrm{Pe}_{\mathrm{SBPSK}} \quad = \quad & \frac{1}{4}Q\left(\sqrt{\frac{\gamma^2 E}{N_0/2}\left\{(1-\lambda)+\frac{2}{T}\int_0^{\frac{\lambda T}{2}}\cos\left(2\pi\int_0^t g(\tau)\,d\tau\right)\,dt\right\}^2}\right) + \\
& \frac{1}{2}Q\left(\sqrt{\frac{\gamma^2 E}{N_0/2}\left\{(1-\frac{\lambda}{2})+\frac{1}{T}\int_0^{\frac{\lambda T}{2}}\cos\left(2\pi\int_0^t g(\tau)\,d\tau\right)\,dt\right\}^2}\right) + \\
& \frac{1}{4}Q\left(\sqrt{\frac{\gamma^2 E}{N_0/2}}\right). \qquad (4.11)
\end{aligned}
$$

In both equations (4.9) and (4.11), the quantity $\frac{\gamma^2 E}{N_0}$ is referred to as the received *signal-to-noise ratio* (SNR).

Figure 4.6 presents probability of error curves obtained from equations (4.9) and (4.11) for BPSK and for various SBPSK signals. It is seen that a relatively small performance penalty results from signal shaping. To measure this penalty, *performance degradation* is defined as the amount of additional SNR, relative to BPSK, required to obtain a desired error probability. For example, 50% D&H SBPSK demonstrates a 1.4 dB degradation at Pe= 10^{-5}, while 50% Min. 3 Term Blackman SBPSK shows only a .5 dB degradation. Clearly, from the analysis presented above, the different

values of Pe for a given SNR are attributable to the differing I channel signal content of the modulations. Those modulations which place more I channel energy into the Q channel have higher probability of error. Comparison of Figures 2.2–2.8 with Figure 4.6 demonstrate this. Note that all SBPSK modulations exhibit performance degradations of 1.4 dB or less at Pe= 10^{-5}.

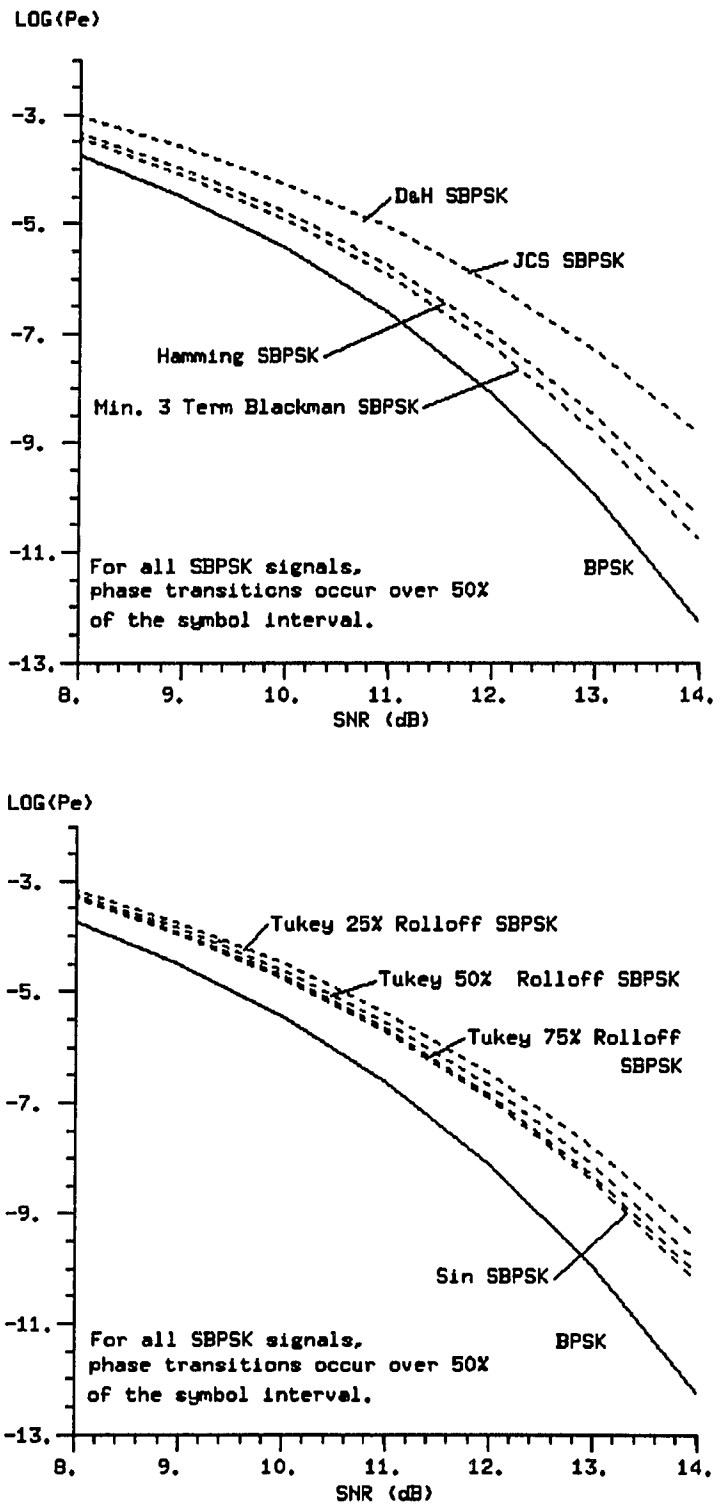

Figure 4.6: Pe for BPSK and Various SBPSK Modulations.

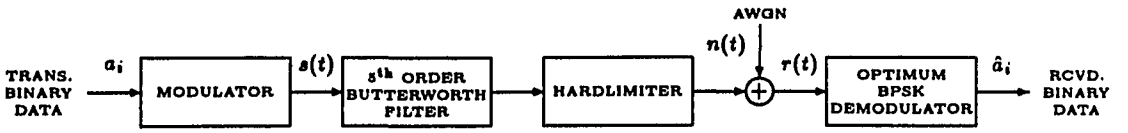

Figure 4.7: A Model of a Typical Satellite Transponder with Downlink AWGN.

4.2 Pe for Bandpass Hardlimited SBPSK

In the previous section, the probability of error for BPSK and SBPSK signals was derived for an infinite bandwidth channel with optimum BPSK demodulation. The channel only attenuated signals and shifted their phase. In this section, probability of error curves obtained from computer simulation are presented for the same signals transmitted through a bandpass hardlimiter, an approximation to a typical satellite transponder. As in Section 3.3, the bandpass hardlimiter was implemented by cascading a fifth order Butterworth filter and a hardlimiter. Zero-mean, stationary, additive white Gaussian noise was applied to the output of the bandpass hardlimiter after which optimum BPSK demodulation was performed. In this way, the performance of BPSK and SBPSK signals transmitted through a typical satellite transponder with downlink AWGN was simulated. Figure 4.7 demonstrates this system. The resulting probability of error curves are presented in Figures 4.8 and 4.9 for one-sided channel bandwidths of R_s Hz and $0.5R_s$ Hz, respectively.

Comparison of Figures 4.6 and 4.8 reveals that bandpass hardlimiting with a channel bandwidth of R_s Hz results in a performance penalty of approximately 0.3 dB at Pe= 10^{-5}, relative to the infinite bandwidth case, for all modulations. In contrast, Figure 4.9 shows that as the channel bandwidth becomes significantly narrow, the performance of different SBPSK modulations and BPSK becomes more similar. When bandpass hardlimited with a channel bandwidth of $0.5R_s$ Hz, 50% D&H SBPSK requires only 0.5 dB more SNR than BPSK to achieve Pe= 10^{-5}. This response is explained below.

For a comfortable channel bandwidth of R_s Hz, all signals are minimally distorted. As a result, the relative performance of the modulations is nearly the same as for the infinite bandwidth channel. However, when the channel bandwidth is reduced to a narrow $0.5R_s$ Hz, the ability of SBPSK signals to absorb the impact of severe bandpass hardlimiting in both the I and Q channels as interphasor crosstalk results in less performance degradation, relative to the infinite bandwidth case, than BPSK. For BPSK, bandpass hardlimiting is entirely absorbed by the I channel signal required for demodulation. In particular, note that for SNR's higher than 11 dB, 50% Min. 3 Term Blackman SBPSK actually has better performance than BPSK when the bandpass hardlimiter bandwidth is $0.5R_s$ Hz.

Figure 4.10 shows the error performance of BPSK and SBPSK signaling as a function of phase reference error for a channel bandwidth of R_s Hz and an 11 dB SNR. While all preceding analysis has assumed perfect carrier phase recovery, it is of interest to determine whether SBPSK signals are particularly sensitive to this "real-world" implementation loss. Examination of this figure reveals that the slopes of the SBPSK curves are minutely greater than the slope of the curve for BPSK. This indicates that SBPSK signals are only slightly more sensitive to phase reference error than BPSK. To obtain values of performance degradation due to a fixed phase reference error, Figure 4.11 is provided. This figure presents Pe curves for a channel bandwidth of R_s Hz and a 10 degree phase reference error. Comparison of Figures 4.8 and 4.11 shows that all modulations exhibit approximately 0.2 dB poorer performance at Pe= 10^{-5}.

Another real world implementation loss is due to non-ideal timing recovery. Dapper and Hill SBPSK is known to be relatively immune to this implementation loss [2]. In [2], Dapper and Hill attribute this to the "mismatch" between the received waveform and the integrate and dump detector. The eye pattern generated by plotting the integrate and dump output versus the recovered symbol time is narrower vertically for SBPSK than for BPSK, but broader in time. The eye is narrower vertically because a portion of the I channel energy is placed in the Q channel for SBPSK. However, it is open for a greater duration of time since the I channel signal does not instantaneously

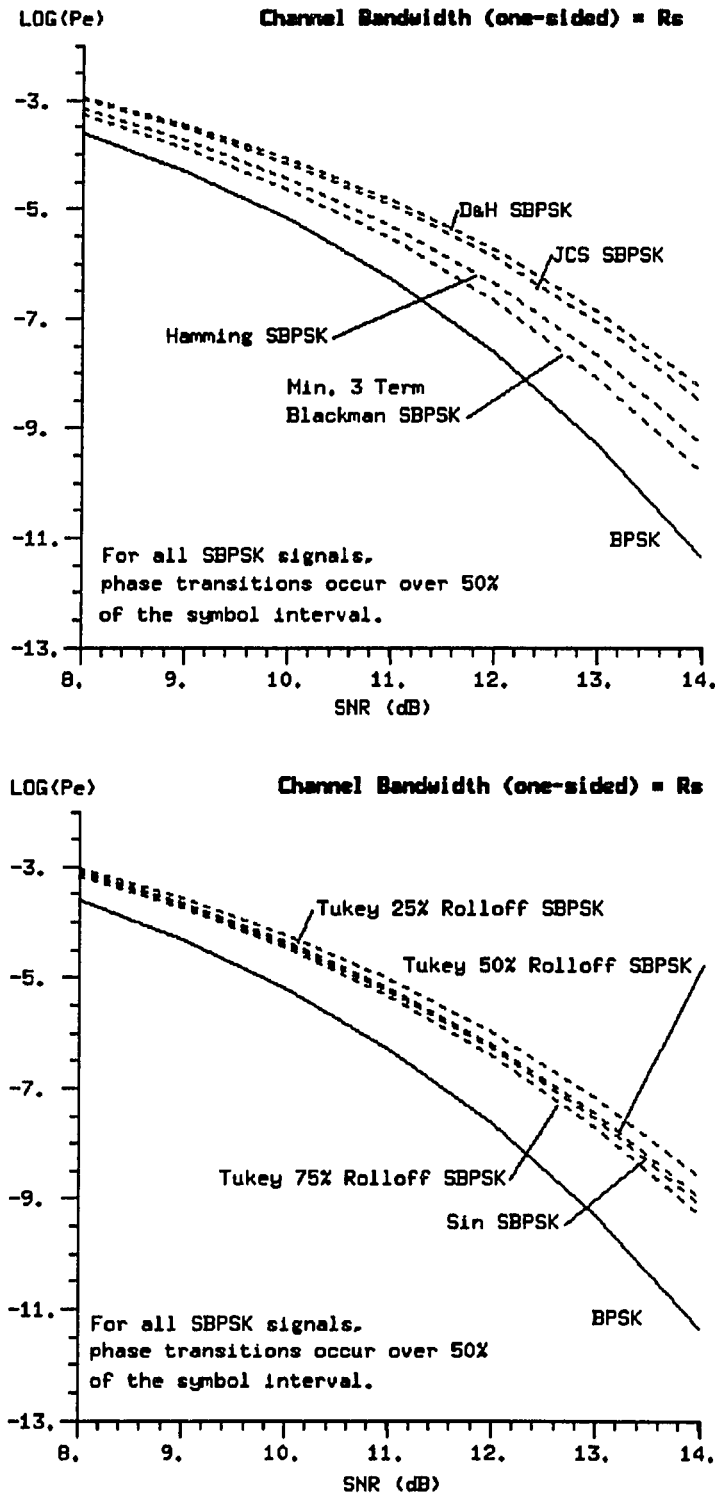

Figure 4.8: Pe for Bandpass Hardlimited BPSK and SBPSK Signals.

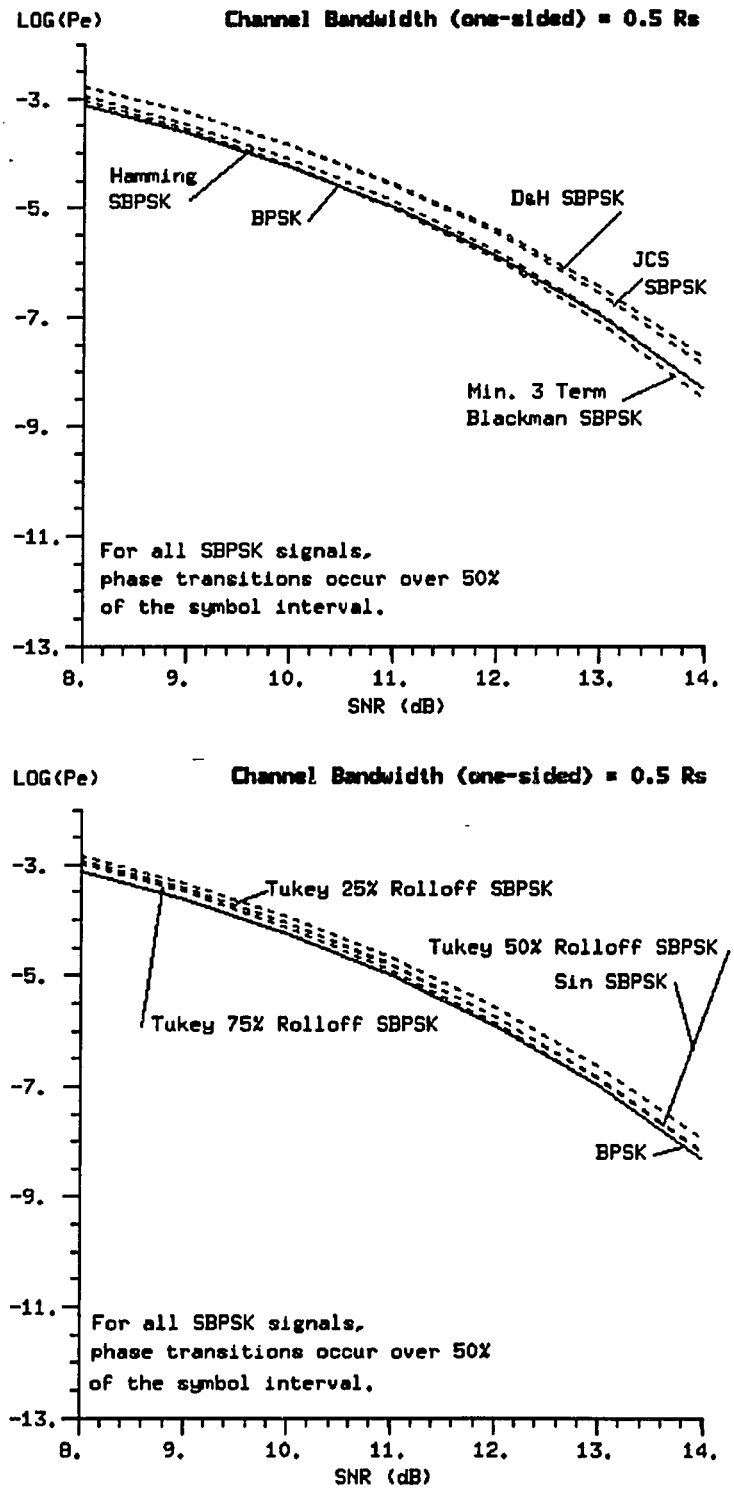

Figure 4.9: Pe for Bandpass Hardlimited BPSK and SBPSK Signals (cont.).

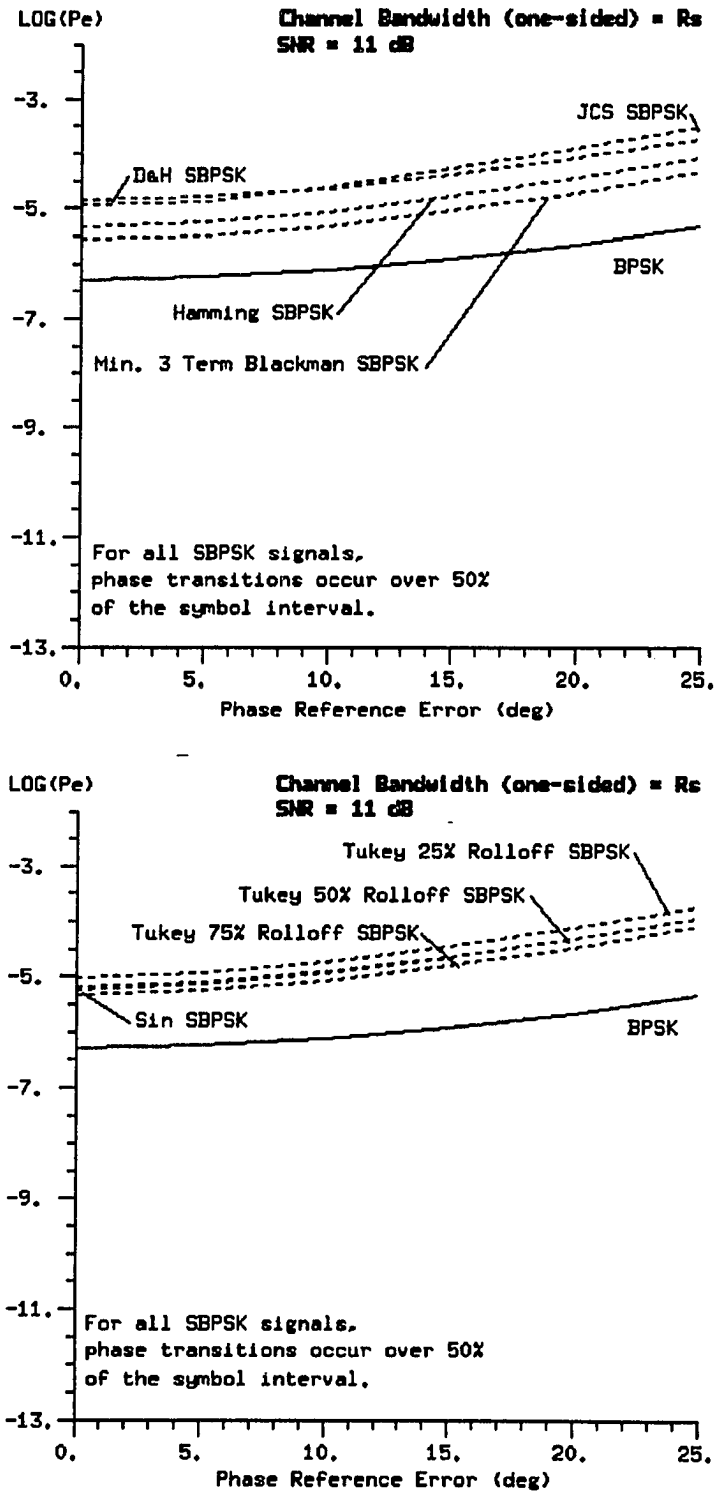

Figure 4.10: Pe vs. Phase Reference Error for Bandpass Hardlimited BPSK and SBPSK Signals.

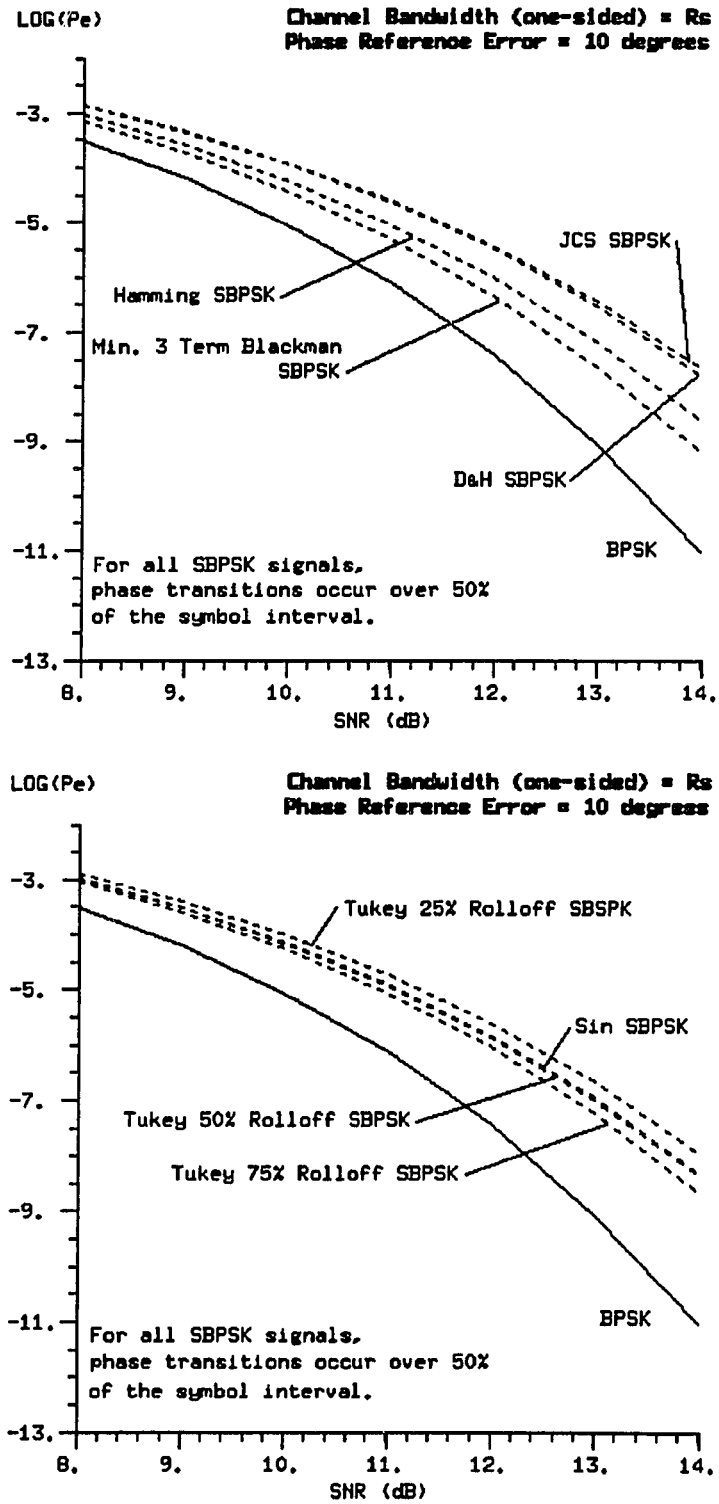

Figure 4.11: Pe for Bandpass Hardlimited BPSK and SBPSK Signals w/ 10° Phase Reference Error.

reverse polarity when data transitions occur. As a result it is expected that SBPSK signals will not demonstrate significantly greater sensitivity to timing jitter than BPSK.

At this point, it is helpful to summarize the results presented in the previous two sections. In Section 4.1, expressions for the probability of error were derived for an infinite bandwidth channel with perfect carrier frequency and phase recovery, as well as ideal symbol timing recovery. In this section, the performance of signals transmitted through a bandpass hardlimiter were investigated. In both cases, 50% Dapper and Hill SBPSK and JCS SBPSK demonstrated the worst performance of the SBPSK modulations examined while 50% Min. 3 Term Blackman SBPSK demonstrated the best performance. In addition, it was shown that as channel bandwidths narrow, error performance becomes more similar. For a channel bandwidth of $0.5R_s$ Hz, all modulations achieve Pe= 10^{-5} with a 0.5 dB range of SNR's. It was also found that SBPSK modulations are not significantly more sensitive to phase reference errors than BPSK, nor is it expected that SBPSK modulations will be significantly more sensitive to timing jitter.

4.3 In-Band Signal-to-Noise Ratio (SNR_I)

In the previous two sections, Figures 4.6–4.11 presented probability of error curves for BPSK and SBPSK signals for a variety of channels. In all but one of these figures, every SBPSK modulation performed worse than BPSK. While this would seem to indicate that SBPSK modulations should not be used, these curves do not reflect the influence of adjacent channel interference (ACI) on performance.

Recall that the motivation for the design and analysis of SBPSK signals is to improve the total utilization of narrowband satellite channels. In this regard, the effects of adjacent channel interference on performance must be accounted for. Clearly, the reduction of out-of-band power for SBPSK signals will result in less adjacent channel interference than BPSK. It follows that lower ACI will at least partially compensate for the degradation in performance caused by signal shaping. To quantify

the simultaneous effects of reduced I channel energy and reduced adjacent channel interference, a new figure of merit is defined.

Let us define SNR_I as the ratio of in-band average I channel energy to twice the power spectral density of the total channel noise. Furthermore, total channel noise is defined as the sum of the background system AWGN with power spectral density $N_0/2$ and noise due to adjacent channel interference. In other words,

$$\begin{aligned} \text{SNR\_I} &= \frac{E_I}{2[N_0/2 + N_{\text{ACI}}/2]} \\ &= \frac{E_I}{N_0 + N_{\text{ACI}}} \end{aligned} \tag{4.12}$$

where E_I is the average in-band I channel energy per bit, $N_0/2$ is the AWGN power spectral density, and $N_{\text{ACI}}/2$ is the average power spectral density of the adjacent channel interference in the channel of interest.

Notice that this expression is analogous to E_b/N_0, the ratio of average total modulation energy per bit to twice the AWGN power spectral density. In fact, if the modulation of interest is BPSK, the channel bandwidth is infinite, and N_{ACI} equal zero due to the complete absence of other channels, SNR_I will equal E_b/N_0. Clearly, for all other cases SNR_I $< E_b/N_0$.

In equation (4.12), the parameter N_0 is determined from the modulation signal-to-noise ratio E_b/N_0, while E_I and N_{ACI} are a function of the specific modulation, the channel bandwidth, and the spacing, number, and psd's of neighboring signals. For the results that will be presented here, the following assumptions were made.

1. There are an infinite number of adjacent channels with equal signal power, equal baud rates, and identical modulation formats (ie: all BPSK, or all 50% D&H SBPSK, etc.).

2. All channels have equal bandwidths with evenly spaced center frequencies as demonstrated in Figure 4.12. In this figure, channel i is the channel of interest and B is the one-sided channel bandwidth.

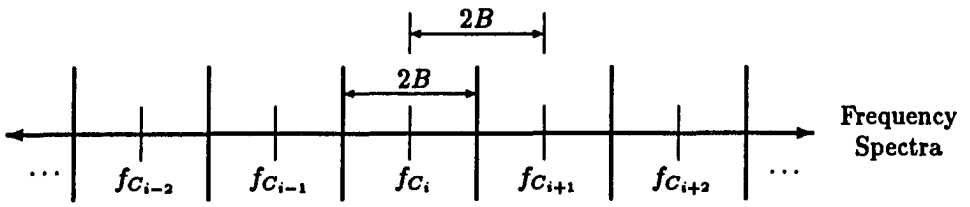

Figure 4.12: Assumed Channel Spacing for Adjacent Channel Interference Analysis.

An additional, underlying assumption is that the average power spectral density of the adjacent channel noise in the bandwidth of interest is white.

It is important to state that error probability cannot be obtained from SNR_I using the Q function. That is, $Pe \neq Q(\sqrt{2 \cdot SNR\_I})$ even though $Pe_{BPSK} = Q(\sqrt{2 \cdot SNR})$. To exactly quantify the relationship between modulation selection, ACI, and error probability, many complex computer simulations are required. In particular, the probability of error would have to be statistically averaged over random parameters such as relative carrier phase offsets and relative symbol timing offsets between adjacent channels. However, it is reasonable to expect that error performance and in-band signal-to-noise ratio are correlated. Consequently, SNR_I should perform well as a figure of merit to rank the relative performance of modulations. Those signals that result in higher SNR_I should also result in better error performance.

Figure 4.13 presents SNR_I as a function of λ, the fraction of the symbol interval for phase transitions, for a one-sided channel bandwidth of R_s Hz and $E_b/N_0 = 9.5$ dB. Notice that BPSK and JCS SBPSK appear as single point values in the figure. By definition, BPSK has instantaneous phase transitions, hence $\lambda = 0$. Similarly, JCS SBPSK was defined only for $\lambda = 0.50$.

For all modulations except Min. 3 Term Blackman SBPSK, SNR_I monotonically increases as λ increases. This demonstrates that at $E_b/N_0 = 9.5$ dB and a channel bandwidth of R_s Hz, the reduction in adjacent channel interference is more significant than the reduction in I channel energy. For Min. 3 Term Blackman SBPSK, a local minimum is observed at $\lambda = 0.15$. Under these conditions, the reduction in ACI is less significant than the reduction in I channel energy due to the

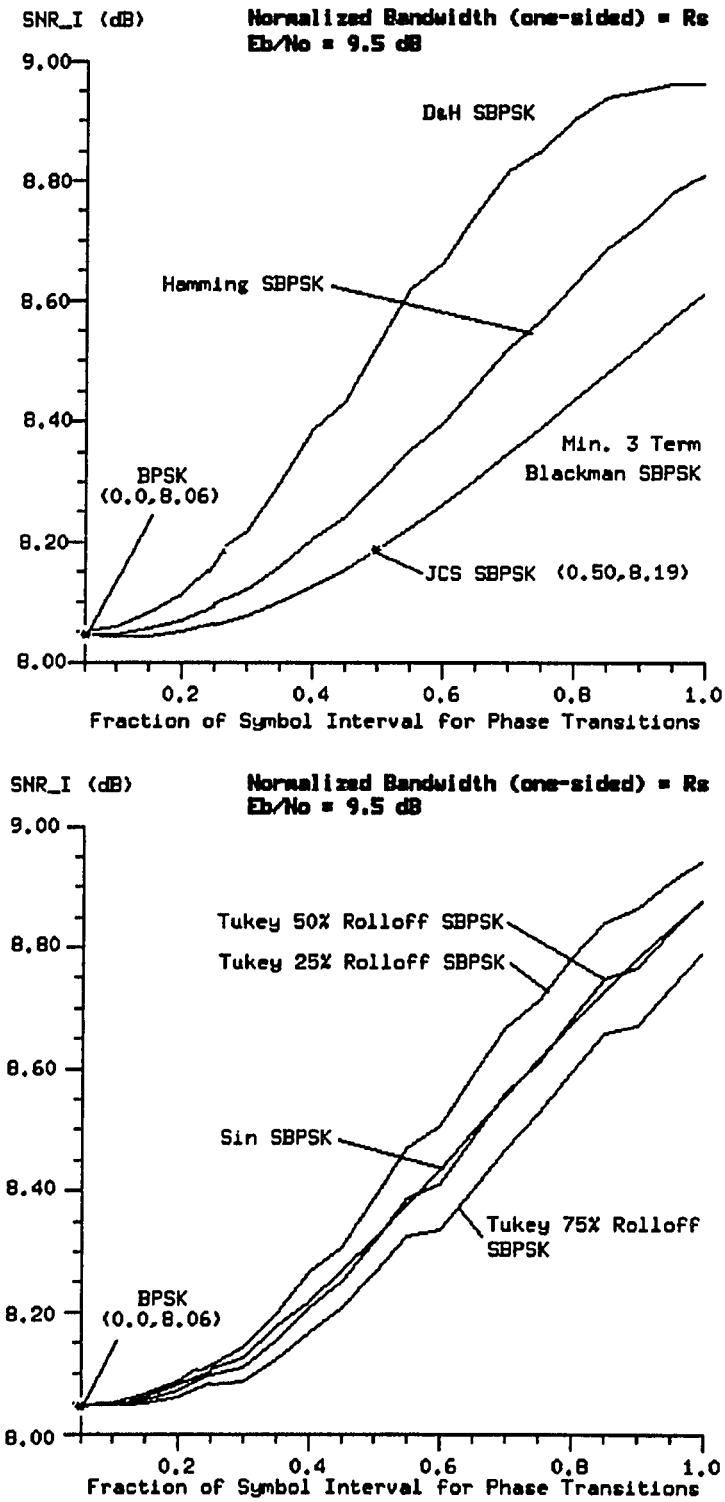

Figure 4.13: SNR_I for BPSK and SBPSK Signals as a Function of λ.

wide mainlobe of this modulation. It is also seen that for every value of λ, D&H SBPSK yields the greatest SNR_I since its out-of-band power is the lowest of all modulations. (See Figure 3.9.)

Although Figure 4.13 shows that SNR_I is the greatest for 100% shaping, only modulations with 50% shaping were analyzed in previous sections since Dapper and Hill report that $\lambda = 0.50$ represents a reasonable limit on this parameter for BPSK compatibility [2]. As λ approaches unity, carrier phase acquisition within conventional BPSK receivers is significantly degraded due to large amounts of Q channel energy. In addition, the duration of phase transitions for JCS SBPSK is consistent with the other SBPSK modulations when $\lambda = 0.50$.

Examination of Figure 4.13 reveals that SNR_I for 50% D&H SBPSK is approximately 0.46 dB greater than SNR_I for BPSK and 0.33 dB greater than SNR_I for JCS SBPSK. Since the inherent similarity of 50% D&H SBPSK and JCS SBPSK results in nearly identical error performance without considering ACI, we may conclude that 50% D&H SBPSK will perform better overall than JCS SBPSK. Such a strong statement cannot be made for BPSK and 50% D&H SBPSK due to restrictions on the implications of SNR_I with respect to error performance. However, it is expected that the performance penalty associated with signal shaping will be considerably lessened when ACI is considered for bandlimited systems.

CHAPTER 5

Summary and Conclusions

5.1 Summary

In Chapter 1, SATCOM 5 kHz channels were identified as satellite links for which the use of new, BPSK interoperable modulations may be appropriate. A brief description of these channels and a list of user restrictions were presented. It was stated that terminals accessing these channels must support a constant amplitude envelope, BPSK interoperable modulation format at a 2400 Hz data rate. In addition, the power spectral density of the transmitted signal must not violate the JCS spectral constraint. This constraint was designed to insure that transmitted signals do not generate adjacent channel interference levels exceeding that of BPSK transmitted at a carrier EIRP of 18 dBW and a 2400 Hz data rate. Finally, Chapter 1 introduced existing BPSK interoperable modulation formats including JCS SBPSK and Dapper and Hill SBPSK.

A new, general class of Shaped BPSK modulations was defined in Chapter 2. It was shown that these signals are a sub-class of the constant amplitude signals and may best be described as BPSK/CPM hybrid modulations. Sets of sample waveforms were presented for several SBPSK modulations.

In Chapter 3, power spectral densities and fractional out-of-band power curves were provided for BPSK and several SBPSK signals. It was seen that JCS SBPSK was the only modulation demonstrating discrete spectral lines. These lines result from the unsymmetric placement of transmitted signals within the complex plane and cause near-violations of the JCS spectral constraint. In contrast, 50% Dapper and Hill SBPSK was shown to allow great flexibility in the choice of transmitter

bit rate and power. In addition, fractional out-of-band power, both before and after bandpass hardlimiting, is lower for 50% D&H SBPSK than for any other modulation examined.

Error performance was the subject of Chapter 4. Expressions for probability of error were derived for BPSK and SBPSK signals transmitted through an infinite bandwidth channel with optimum BPSK demodulation. Simulations were performed to analyze the error probability of bandpass hardlimited signals and to examine the effects of implementation losses. For both the infinite bandwidth channel and the bandpass hardlimiter, JCS SBPSK and 50% D&H SBPSK demonstrated the worst error performance of the signals examined. However, as channel bandwidths narrow, differences in error performance diminish. In addition, it was shown that SBPSK signals are not significantly more sensitive to phase reference errors than BPSK, nor is it expected that they are significantly more sensitive to timing jitter. Finally, to quantify the simultaneous reduction of I channel energy and adjacent channel interference resulting from signal shaping, a new figure of merit was defined. When E_b/N_0 equals 9.5 dB and the channel bandwidth is R_s Hz, SNR_I is greatest for D&H SBPSK because this modulation causes the least adjacent channel interference. It is expected that the reduced adjacent channel interference of D&H SBPSK will substantially reduce the degradation in error performance that results from signal shaping.

The remaining two sections of this chapter are devoted to suggestions for further research and the recommendation of a SBPSK signal for experimental applications.

5.2 Topics for Future Research

In this research, many issues have been addressed in an attempt to obtain a basic understanding of the attributes and performance of Shaped BPSK signals. Some of these topics provide excellent areas for further investigation. For example, all power spectral densities presented in Chapter 3 were obtained from computer simulation. Future work may provide analytic solutions for specific pulse shapes or a general semi-analytic solution for all SBPSK modulations. This solution might

then be "customized" for specific pulse shapes. Other areas of interest include analytic analysis of the performance degradation caused by bandlimiting, phase reference errors, symbol timing errors, or other implementation losses.

The design of an optimum demodulator for SBPSK signals and the optimum SBPSK error performance are of particular interest. As a result of the inherent spectral efficiency of these modulations, it may be found that SBSPK signaling performs significantly better than BPSK under bandlimited conditions. In addition, optimally demodulated SBPSK signals would almost certainly perform better than BPSK when adjacent channel interference effects are accounted for.

Finally, the performance of SBPSK signals transmitted through a non-linear device with adjacent channel interference and AWGN present at the input is of the greatest interest. Intermodulation and power sharing can cause significant degradation to the signal of interest under these conditions. This model would accurately predict the performance of these signals in real-world satellite communication systems.

5.3 Recommended SBPSK Waveform

In a memorandum to the Joint Chiefs of Staff of the United States Department of Defense, C. E. McKnight recommends a BPSK interoperable modulation we have referred to as JCS SBPSK [1]. The motivation for this is to effectively bandlimit BPSK while retaining a constant amplitude signal envelope. The underlying presumption is that significant bandlimiting improves the total utilization of the narrowband 5 kHz SATCOM channels, even though the I channel energy required for BPSK interoperability is reduced.

In this work, we have investigated many Shaped BPSK modulations and compared various properties. We have found that 50% Dapper and Hill SBPSK provides greater bandlimiting than JCS SBPSK with exactly the same loss in I channel energy. While it was also found that SBPSK modulations with smoother pulse shapes demonstrate less I channel energy loss, they also demonstrate

less bandlimiting and thus greater adjacent channel interference. We therefore recommend the further investigation of 50% Dapper and Hill SBPSK for use with 5 kHz SATCOM channels. The advantages of Dapper and Hill SBPSK are summarized below.

1. The average Q channel signal for JCS SBPSK is non-zero. This is not true for all the other modulations studied, including Dapper and Hill SBPSK. This is significant since a Q channel offset will disturb the phase error measurement of the Costas or squaring loops found in many BPSK demodulators.

2. The power spectral density of JCS SBPSK exhibits discrete spectral lines at integer multiples of the transmitted symbol rate. These lines may result in false-lock in the carrier acquisition circuitry of neighboring channels. In contrast, D&H SBPSK demonstrates spectral nulls at these locations.

3. The power spectrum of 50% D&H SBPSK is well "matched" to the JCS spectral constraint. This allows great flexibility in the choice of transmitter power and bit rate. At a carrier EIRP of 18 dBW, 50% D&H SBPSK may be transmitted at 3600 bits per second (bps) while easily conforming to the JCS spectral constraint. Alternatively, this modulation may be transmitted at a carrier EIRP of 22 dBW when the data rate is 2400 bps.

4. 50% Dapper and Hill SBPSK has the lowest fractional out-of-band power and adjacent channel interference of any SBPSK modulation investigated for narrowband channels (one-sided channel bandwidth $< 2.5R_s$ Hz.) At the required data rate of 2400 bps, the 4 kHz nominal passband bandwidth of the 5 kHz SATCOM channels may be equivalently expressed as $0.83R_s$ Hz (one-sided). For this value of channel bandwidth, 50% D&H SBPSK demonstrates 1.4 dB less fractional out-of-band power than BPSK. It is expected that the reduction in adjacent channel interference for 50% D&H SBPSK will compensate for the approximate 1 dB performance penalty (relative to BPSK) it exhibits when bandpass hardlimited with a channel bandwidth of $0.83R_s$ Hz. This is demonstrated by SNR_I, a figure of merit that quantifies

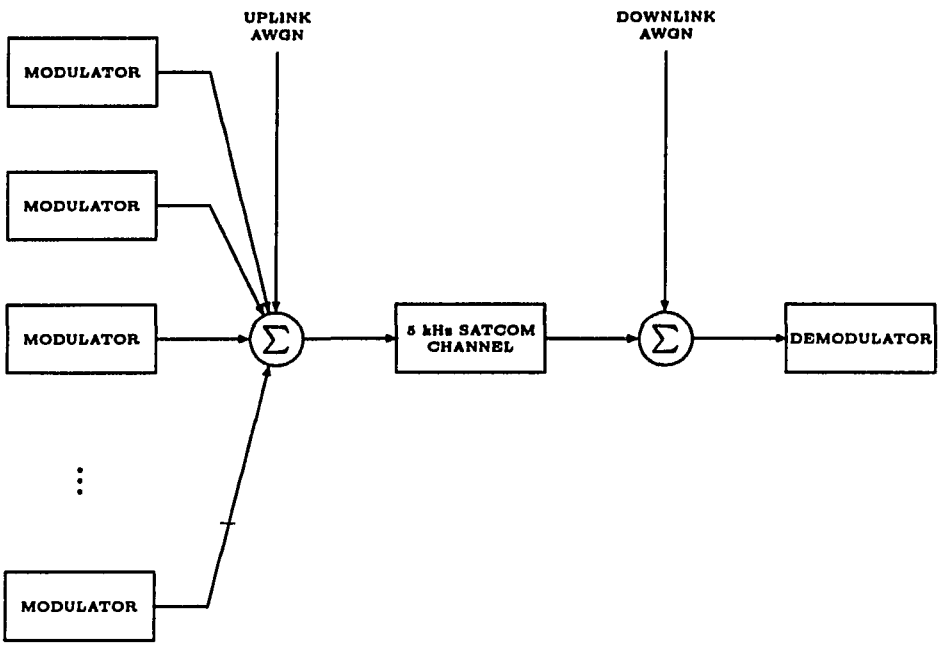

Figure 5.1: Complete 5 kHz SATCOM Channel System.

the simultaneous reduction in both I channel energy and adjacent channel interference. When $E_b/N_0 = 9.5$ dB and the channel bandwidth is R_s Hz, SNR_I for 50% D&H SBPSK is 0.46 dB greater than that of BPSK and 0.33 dB greater than that of JCS SBPSK.

To obtain exact system performance information, the system in Figure 5.1 would have to be simulated, or experimentation with system hardware would have to be performed. These simulations were not performed here since 5 kHz SATCOM channel information is not available in the literature. In addition, relative frequency offsets of the modulator carrier frequencies dictate that these simulations cannot be performed at baseband. As a result, considerable computing power would be necessary.

In conclusion, we recommend experimental use of 50% Dapper and Hill SBPSK. This modulation should generally perform better than JCS SBPSK. To insure that the reduction in adjacent channel interference does compensate for the reduction of I channel energy, we recommend that the experimental results obtained for 50% D&H SBPSK be compared with those of BPSK under similar conditions.

REFERENCES

[1] C. E. McKnight, Jr., "Technical Criteria for UHF SATCOM Terminals Accessing Nonprocessed Satellite Channels." Memorandom for The Joint Chiefs of Staff, Washington D.C., MJC-33-87, (typewritten), Mar. 1987.

[2] M. J. Dapper and T. J. Hill, "SBPSK: A Robust Bandwidth-Efficient Modulation for Hard-limited Channels," in *MILCOM '84. IEEE Military Comm. Conf. Conference Record (Cat. No. 84CH2069-3)*, vol. 3, pp. 458–463, Oct. 1984.

[3] H. Yazdani, K. Feher, and W. Steenhart, "Constant Envelope Bandlimited BPSK Signal," *IEEE Trans. Commun.*, vol. COM-28, pp. 889–897, June 1980.

[4] C. Sundberg, "Continuous Phase Modulation," *IEEE Communications Magazine*, vol. 24, pp. 25–38, Apr. 1986.

[5] J. Anderson, T. Aulin, and C.-E. Sundberg, *Digital Phase Modulation.* New York, NY: Plenum Publishing Company, 1986.

[6] T. Aulin, *CPM—A Power and Bandwidth Efficient Digital Constant Envelope Modulation Scheme.* PhD thesis, University of Lund, Lund, Sweden, Nov. 1979.

[7] T. Aulin and C.-E. Sundberg, "Continuous Phase Modulation—part I: Full Response Signaling," *IEEE Trans. Commun.*, vol. COM-29, pp. 196–209, Mar. 1981.

[8] T. Aulin, N. Rydbeck, and C.-E. Sundberg, "Continuous Phase Modulation—part II: Partial Response Signaling," *IEEE Trans. Commun.*, vol. COM-29, pp. 210–225, Mar. 1981.

[9] T. Aulin and C.-E. Sundberg, "CPM—An Efficient Constant Amplitude Modulation Scheme," *International Journal of Satellite Communications*, vol. 2, pp. 161–186, Jul.–Sep. 1984.

[10] J. B. Anderson, C.-E. Sundberg, T. Aulin, and N. Rydbeck, "Power-Bandwidth Performance of Smoothed Phase Modulation Codes," *IEEE Trans. Commun.*, vol. COM-29, pp. 187–195, Mar. 1981.

[11] F. Harris, "On the Use of Windows for Harmonic Analysis with the Discrete Fourier Transform," *Proceedings of the IEEE*, vol. 66, pp. 51–83, Jan. 1978.

[12] R. R. Anderson and J. Salz, "Spectra of Digital FM," *Bell Syst. Tech. Jour.*, vol. 44, pp. 1165–1189, Jul.–Aug. 1965.

[13] V. K. Prabhu and H. E. Rowe, "Spectra of Digital Phase Modulation by Matrix Methods," *Bell Syst. Tech. Jour.*, vol. 53, pp. 899–932, May–Jun. 1974.

[14] V. K. Prabhu, "Spectral Occupancy of Digital Angle-Modulated Signals," *Bell Syst. Tech. Jour.*, pp. 429–453, Apr. 1976.

[15] H. E. Rowe and V. K. Prabhu, "Power Spectrum of a Digital Frequency-Modulated Signal," *Bell Syst. Tech. Jour.*, vol. 53, pp. 1095–1125, Jul.–Aug. 1975.

[16] T. J. Baker, "Asymptotic Behavior of Digital FM Spectra," *IEEE Trans. Commun.*, vol. COM-22, pp. 1585–1589, Oct. 1974.

[17] G. J. Garrison, "A Power Spectral Density Analysis for Digital FM," *IEEE Trans. Commun.*, vol. COM-23, pp. 1228–1243, Nov. 1975.

[18] T. Aulin and C.-E. Sundberg, "Exact Asymptotic Behavior of Digital FM Spectra," *IEEE Trans. Commun.*, vol. COM-30, pp. 2438–2449, Nov. 1982.

[19] G. L.Pierobon, S. G. Pupolin, and G. P. Tronca, "Power Spectrum of Angle Modulated Correlated Digital Signals," *IEEE Trans. Commun.*, vol. COM-30, pp. 389–395, Feb. 1982.

[20] T. Aulin and C.-E. Sundberg, "Calculating Digital FM Spectra by Means of Autocorrelation," *IEEE Trans. Commun.*, vol. COM-30, pp. 1199–1208, May 1982.

[21] T. Aulin and C.-E. Sundberg, "An Easy Way to Calculate Power Spectrum of Digital FM," *IEE Proc., Part F, Communications, Radar and Signal Processing*, vol. 130, pp. 519–526, Oct. 1983.

[22] T. Aulin, G. Lindell, and C.-E. Sundberg, "Selecting Smoothing Pulses for Partial Response Digital FM," *IEE Proc., Part F, Communications, Radar and Signal Processing*, vol. 128, pp. 237–244, Aug. 1981.

[23] S. G. Wilson and R. C. Gauss, "Power Spectra of Multi-h Phase Codes," *IEEE Trans. Commun.*, vol. COM-29, pp. 250–256, Mar. 1981.

[24] L. F. Lind and A. A. deAlbuquerque, "Special Calculation of Partial Response Multi-h Codes," *Electronics Letters*, vol. 17, pp. 713–717, Oct. 1981.

[25] F. Amoroso, "Pulse and Spectrum Manipulation in the Minimum (frequency) Shift Keying (MSK) Format," *IEEE Trans. Commun.*, vol. COM-24, pp. 381–384, Mar. 1976.

[26] M. K. Simon, "A Generalization of Minimum-Shift-Keying (MSK)-type Signaling Based Upon Input Data Symbol Pulse Shaping," *IEEE Trans. Commun.*, vol. COM-24, pp. 845–856, Aug. 1976.

[27] I. Sasase, K. Feher, and S. Mori, "Asymmetrical Pulse Shaped QPSK Modulation Systems," *IEEE Trans. Commun.*, vol. COM-33, pp. 1146–1150, Oct. 1985.

[28] I. Sasase, S. Mori, and K. Feher, "Bandwidth Efficient Modulation Technique by Asymmetrical Pulse Shaping," in *Communications in the Information Age (Cat. No. 84CH2064-4)*, Atlanta, GA, pp. 1086–1090, IEEE Global Telecommunications Conference, GLOBECOM '84, Nov. 1984.

[29] P. Ho, *The Power Spectral Density of Digital Continuous Phase Modulation with Correlated Data Symbols.* PhD thesis, Queen's University, Kingston, Ontario, Canada, Aug. 1985.

[30] J. G. Proakis, *Digital Communications.* McGraw-Hill Book Company, 1989.

[31] E. Biglieri and M. Visintin, "A Simple Derivation of the Power Spectrum of Full-Response CPM and Some of its Properties," *IEEE Trans. Commun.*, vol. 38, pp. 267–269, Mar. 1990.

[32] K. Feher, *Digital Communications: Satellite/Earth Station Engineering.* Englewood Cliffs, NJ: Prentice-Hall Inc., 1983.